International
Progress Report

IPR-04-33

Äspö Hard Rock Laboratory

Äspö Task Force

PA calculations for feature A with third-dimention structure based on tracer test calibration

Christine Doughty, LBNL

Masahiro Uchida, JNC

January 2003

Svensk Kärnbränslehantering AB
Swedish Nuclear Fuel
and Waste Management Co
Box 5864
SE-102 40 Stockholm Sweden
Tel 08-459 84 00
+46 8 459 84 00
Fax 08-661 57 19
+46 8 661 57 19

Äspö Hard Rock
Laboratory

Report no.
IPR-04-33
No.
F65K
Author
Christine Doughty
Masahiro Uchida
Date
Jan 2003
Checked by
Masahiro Uchida
Date
July 2004
Approved
Christer Svemar
Date
2004-08-30

Äspö Hard Rock Laboratory

Äspö Task Force

PA calculations for feature A with third-dimention structure based on tracer test calibration

Christine Doughty, LBNL

Masahiro Uchida, JNC

January 2003

Keywords: Transport modeling, particle-tracking coupled with analytical solution, spatial permeability variations over fracture plane, flow distribution among sub-fractures, matrix diffusion, sorption, fracture filling, splay fractures, unaltered rock, site characterization, performance assessment, THEMM, TRUE-1 site

Abstract

A new method has been applied to model flow and transport within a complex fracture zone at the TRUE-1 site. The method accounts for advection through the fractures themselves and diffusion and sorption into fracture infill and other surrounding materials. The flow and transport simulator THEMM is employed to calculate transport processes, using a particle-tracking approach coupled with an analytical solution for fracture-matrix diffusion and sorption. The fracture is modeled using a two-dimensional heterogeneous transmissivity distribution, with residence times adjusted to account for structure in the third dimension (the fracture-zone thickness). Model parameters that are not well constrained by available data are inferred from calibration to the STT-1b tracer test. Preliminary results show that for performance assessment boundary conditions, the time required to traverse 10 m across the model varies by orders of magnitude among tracers with different sorption strengths, indicating that diffusion and sorption significantly retard tracer transport. Sensitivity studies illustrate how tracer breakthrough curves are affected by fracture-zone flow partitioning among large and small sub-fractures, and the relative proportions of different materials present.

Sammanfattning

En ny metod har applicerats för att modellera flöde och transport i en komplicerad sprickzon vid platsen för TRUE-1. Metoden tar hänsyn till advektion i sprickor samt diffusion och sorption på sprickfyllnadsmaterial eller omgivande material. Flödes- och transportsimulatorn THEMM har använts för att beräkna transportprocesser, genom att använda en partikelspårningsteknik kopplad till en analytisk lösning för matrisdiffusion och sorption. Sprickan är modellerad som en tvådimensionell heterogen transmissivitetsfördelning uppehållstider justerade med hänsyn till den tredje dimensionen (sprickzonens tjocklek). Modellparametrar som inte är välbestämda genom tillgängliga data har antagits genom kalibrering mot spårförsöket STT-1b. Preliminära resultat visar att matrisdiffusion och sorption kan ha en stor inverkan under naturliga förvarsrandvillkor. Även för en 10 m lång spricka varierar transporttiderna flera storleksordningar för ämnen med olika sorptionsstyrkor. Känslighetsanalyser visar hur uppdelningen av flödet mellan stora och små sprickor påverkar genombrottskurvor. Även effekten av olika förhållanden mellan olika sprickmaterial har studerats.

Executive summary

The key flow and transport processes occurring in a complex fracture zone such as Feature A are advection, dispersion, diffusion, and sorption. The key factors affecting how and where these processes occur, illustrated in Figure 1, are spatial permeability variations over the plane of the fracture zone (the x-y plane in Figure 1); multiple sub-fractures within the fracture zone thickness (the z direction in Figure 1, where two sub-fractures are shown); gouge materials within each of the sub-fractures; splays, or minor fractures, in between the two sub-fractures that break up the rock into blocks of sizes a fraction of the width of the complex fracture; dead-end pores and splays into neighboring rocks; and unaltered rock surrounding the fracture zone. We apply a new modeling approach that has recently been developed to model these processes in complex fracture zones (Tsang and Doughty, 2002).

Model development begins with the generation of a two-dimensional (2D) heterogeneous fracture-transmissivity distribution. We then use a finite-difference code to calculate the 2D fluid flow field q(x,y) through the fracture for a given set of boundary conditions (either a tracer test or natural gradient). We account for structure in the third dimension (the fracture zone thickness) by assuming that there are two sub-fractures in a ladder-like structure (Figure 1). We assume that at each (x,y) location: (1) the flow q(x,y) represents the sum of the flow in the two sub-fractures: $q_1 + q_2 = q$; (2) q, q_1 and q_2 are in the same direction; and (3) the ratio of flow between sub-fractures 1 and 2 is $\alpha = q_2/q_1$, where the parameter α is denoted the fracture structure parameter. Diffusion and sorption into the materials surrounding the sub-fractures are conceptualized as occurring in three matrix-block populations with different characteristic sizes: small (gouge material infilling the sub-fractures), intermediate (matrix blocks within the ladder structure), and large (the semi-infinite rock matrix outside the ladder structure).

Model parameters that are not well constrained by available data are inferred from calibration to the breakthrough curve from the STT-1b tracer test. Good agreement is obtained for the non-sorbing tracers (HTO and I) by varying the heterogeneity of the fracture-transmissivity distribution, the fracture porosity, the relative proportion of small matrix blocks (gouge), and the fracture structure parameter α. Reasonable matches to the breakthrough behaviour for sorbing tracers (Sr, Co, and Tc) are obtained by increasing their sorption strength in the gouge material.

Preliminary results show that for performance assessment boundary conditions, the time required to traverse 10 m across the model is less than one month in the absence of any diffusion or sorption effects (transport solely by advection through the fracture network) and ranges from five months to 16,000 years for tracers with different sorption strengths, indicating that diffusion and sorption significantly retard tracer transport. Sensitivity studies illustrate how tracer breakthrough curves can develop double-humped shapes as a result of fracture-zone flow partitioning among large and small sub-fractures.

Contents

List of tables

List of figures

1 Introduction

Nearly all of the studies of flow and transport in fractures have assumed that each fracture can be modeled as an open space between two surfaces with constant or variable separation. Recent studies of rock fractures have shown that a fracture in the field can be much more complex, consisting of a thin fracture zone having several interconnected sub-fractures through which advection occurs. Additionally, fracture zones include dead-end sub-fractures and stagnant pore space, highly porous fault gouge materials that partially fill sub-fractures, small matrix blocks within the fracture zone, and the rock matrix adjacent to the fracture zone, which all provide material in which solute diffusion and sorption can occur. We take a new approach to modeling flow and transport within a complex fracture or fracture zone (Tsang and Doughty, 2002) that addresses all these features, and apply it to tracer transport in Feature A at the TRUE site of the Äspö Hard Rock Laboratory.

2 Modeling Tasks

Task 6 seeks to provide a bridge between site characterization (SC) and performance assessment (PA) approaches to modeling solute transport in fractured rock. Both SC-type and PA-type models are applied to tracer transport, considering experimental boundary conditions (Task 6A) and boundary conditions for a PA scale (Task 6B, 6B2). In Task 6a, we attempt to reproduce some of the results from Äspö *in situ* tracer experiment STT-1b, by varying model parameters that are not well constrained by available data. The model itself is not changed for Tasks 6b and 6b2, but boundary conditions specified for PA modeling are applied.

2.1 Task 6A

The task consists of modeling selected tracers used in the STT-1b test performed within the TRUE-1 program. The test was conducted using two packed off boreholes penetrating a water-conducting fracture zone (Feature A) with a roughly planar structure about 2 cm thick and an assumed lateral extent of 15 m by 15 m. The two boreholes intersect Feature A about 5 m apart. The injection flow rate accompanying tracer release is much smaller than the production flow rate accompanying tracer capture, so the flow field is nominally radial. Tracers range from non-sorbing to strongly sorbing. Modelers were provided with site characterization data, data from preliminary tracer tests with non-sorbing tracers, laboratory measurements of retention parameters (D_e, K_a and K_d) and were asked to predict drawdown at the boreholes and tracer breakthrough.

2.2 Task 6B

The task consists of modeling the selected tracers used in the STT-1b test performed within the TRUE-1 program with PA-relevant time scales. Task 6B is defined in such a way that flow and transport will occur in the same pathway as in the STT-1b test. This is achieved by employing the same borehole intervals intersecting Feature A as in Task 6A, but by decreasing the injection and production rates by a factor of 1000. Modelers were asked to predict tracer breakthrough for a constant tracer injection and a pulse tracer injection.

2.3 Task 6B2

The task consists of modeling the selected tracers used in the STT-1b test performed within the TRUE-1 program with new PA-relevant boundary conditions and time scales. Task 6B2 is defined in such a way that flow and transport will occur over a larger part of Feature A than during the STT-1b test. A head difference is imposed on two opposite sides of the model and the remaining two sides are considered closed, establishing a nominally linear flow field. Tracer is released along a 2-m long line oriented perpendicular to the flow direction, located 5 m from the upgradient boundary of the model. Tracer is collected over the entire downgradient boundary of the model. Modelers were asked to predict tracer breakthrough for a constant tracer injection and a pulse tracer injection.

3 Model description

The key flow and transport processes occurring in a complex fracture zone such as Feature A are advection, dispersion, diffusion, and sorption. The key factors affecting how and where these processes occur, illustrated in Figure 1, are spatial permeability variations over the plane of the fracture zone (the x-y plane in Figure 1); multiple sub-fractures within the fracture zone thickness (the z direction in Figure 1, where two sub-fractures are shown); gouge materials within each of the sub-fractures; splays, or minor fractures, in between the two sub-fractures that break up the rock into blocks of sizes a fraction of the width of the complex fracture; dead-end pores and splays into neighboring rocks; and unaltered rock surrounding the fracture zone. We apply a new modeling approach that has recently been developed to model these processes in complex fracture zones (Tsang and Doughty, 2002).

Model development begins with the generation of a two-dimensional (2D) heterogeneous fracture-transmissivity distribution. We then use a finite-difference code to calculate the 2D fluid flow field q(x,y) through the fracture for a given set of boundary conditions (either a tracer test or natural gradient). We account for structure in the third dimension (the fracture zone thickness) by assuming that there are two sub-fractures in a ladder-like structure (Figure 1). We assume that at each (x,y) location: (1) the flow q(x,y) represents the sum of the flow in the two sub-fractures: $q_1 + q_2 = q$; (2) q, q_1 and q_2 are in the same direction; and (3) the ratio of flow between sub-fractures 1 and 2 is $\alpha = q_2/q_1$. The parameter α is denoted the fracture structure parameter. Diffusion and sorption into the materials surrounding the sub-fractures are conceptualized as occurring in three matrix-block populations with different characteristic sizes: small (gouge material infilling the sub-fractures), intermediate (matrix blocks within the ladder structure), and large (the semi-infinite rock matrix outside the ladder structure). Each of these steps is described more fully in the following sections.

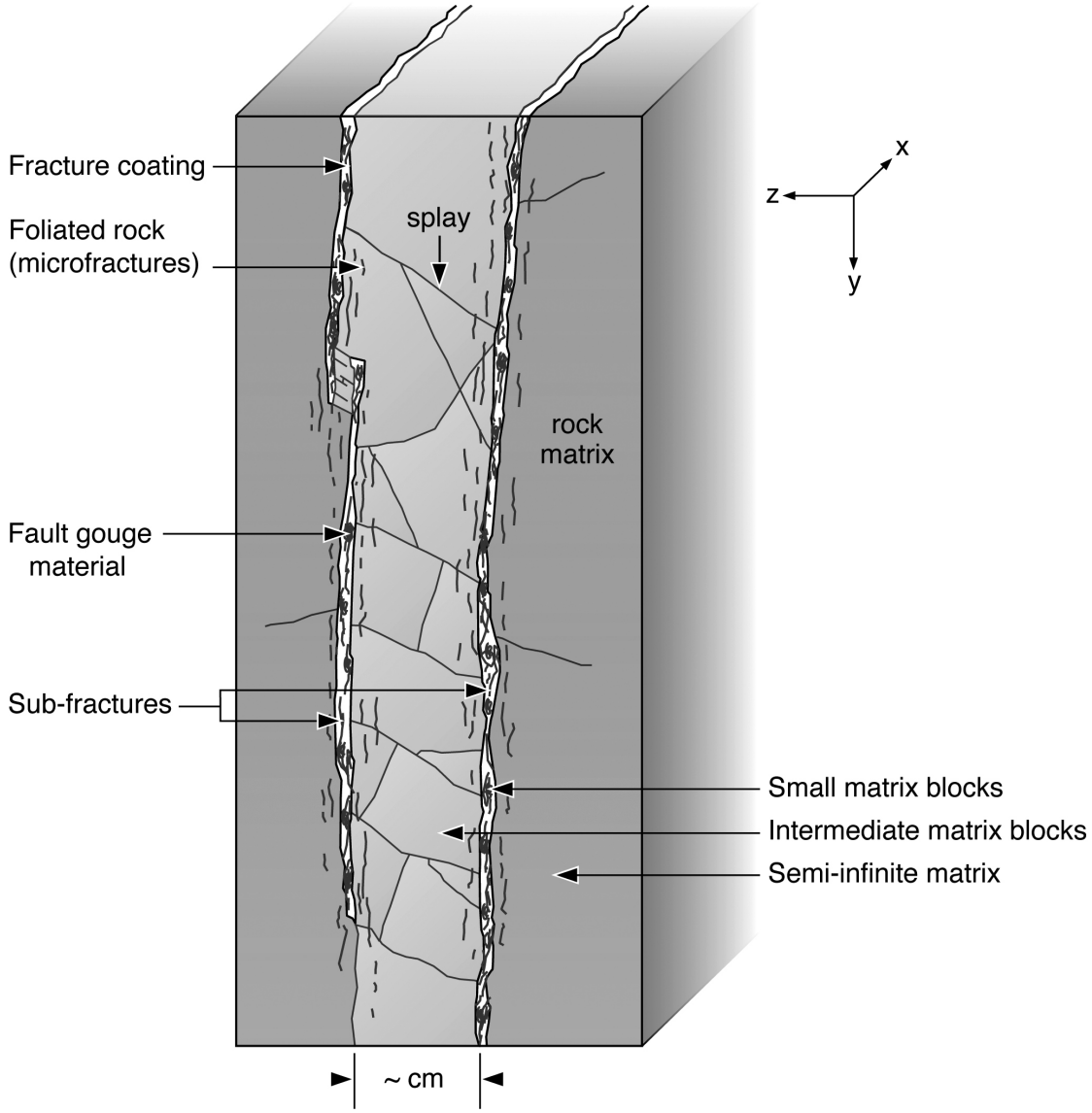

Figure 1. *Structure of a complex fracture or master fault (adapted from Mazurek et al., 2001).*

3.1 Transmissivity distribution and 2D flow field

Figure 2 shows the distribution of transmissivities obtained from a series of well tests using packers to isolate Feature A (Table 2-1, Task 6B2 Modeling task specification). The distribution is interpreted as bimodal, and in keeping with the notion that higher-transmissivity fractures tend to be more extensive, transmissivities above a threshold level are assigned a longer correlation length than transmissivities below it. The geostatistical program SISIM (Deutsch and Journel, 1998) uses the cumulative distribution function (CDF) shown in Figure 2 and user-specified variogram parameters to generate heterogeneous transmissivity distributions. Figure 3 shows two isotropic transmissivity (T) fields generated by SISIM, along with the flow field obtained by

imposing a head difference between the top and bottom boundaries of the model and taking the side boundaries of the model as closed. The T field shown in Figure 3a is based directly on the CDF shown in Figure 2, and yields a mean value of $\log_{10}T = -7.5$ and a standard deviation of $\sigma_{\log 10T} = 0.58$. The T field shown in Figure 3b uses a rescaled CDF ranging from $-8.8 < \log_{10}T < -5.4$, producing a more strongly heterogeneous field with the same mean but a larger standard deviation of $\sigma_{\log 10T} = 1.38$. The degree of channeling and preferential flow is clearly much greater in the more heterogeneous transmissivity field.

Figure 4 shows two anisotropic transmissivity fields generated by SISIM, based directly on the CDF shown in Figure 2. Despite the longer correlation lengths, the flow fields (not shown) show about the same amount of preferential flow as that shown in the Figure 3a transmissivity distribution, based on Figure 2. Although the transmissivity fields shown in Figure 4 look plausible, we believe that there is not sufficient field evidence to support the use of an anisotropic transmissivity field for Feature A. Therefore, we use isotropic fields such as those shown in Figure 3, with the mean and standard deviation determined by calibration to STT-1b tracer test data.

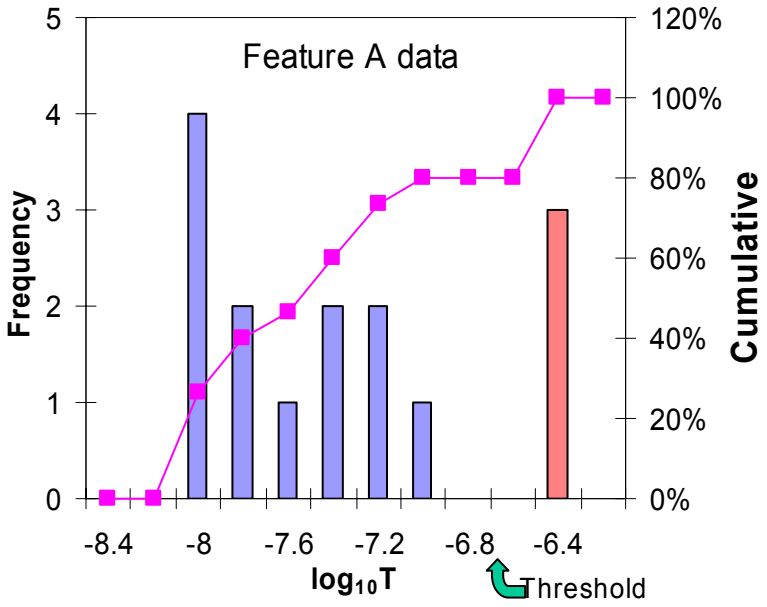

Figure 2. *Histogram of transmissivity values obtained from well tests conducted on Feature A. The CDF is used by SISIM to generate heterogeneous transmissivity fields.*

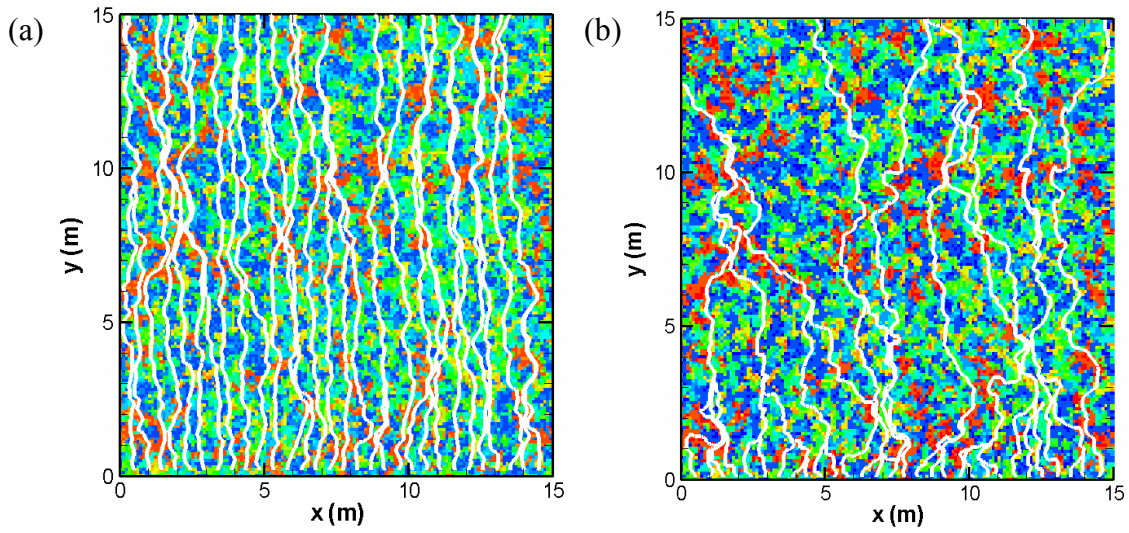

Figure 3. *Heterogeneous, isotropic transmissivity fields generated by SISIM (red is high T, blue is low T). A 1 m long correlation length is specified for T values above the threshold and a 0.3 m long correlation length is specified for T values below the threshold. The field in (a) is based directly on the CDF shown in Figure 2. The field in (b) uses a rescaled CDF ranging from* $-8.8 < \log_{10}T < -5.4$. *The white lines are streamlines illustrating the flow fields obtained by imposing a head difference between the top and bottom model boundaries.*

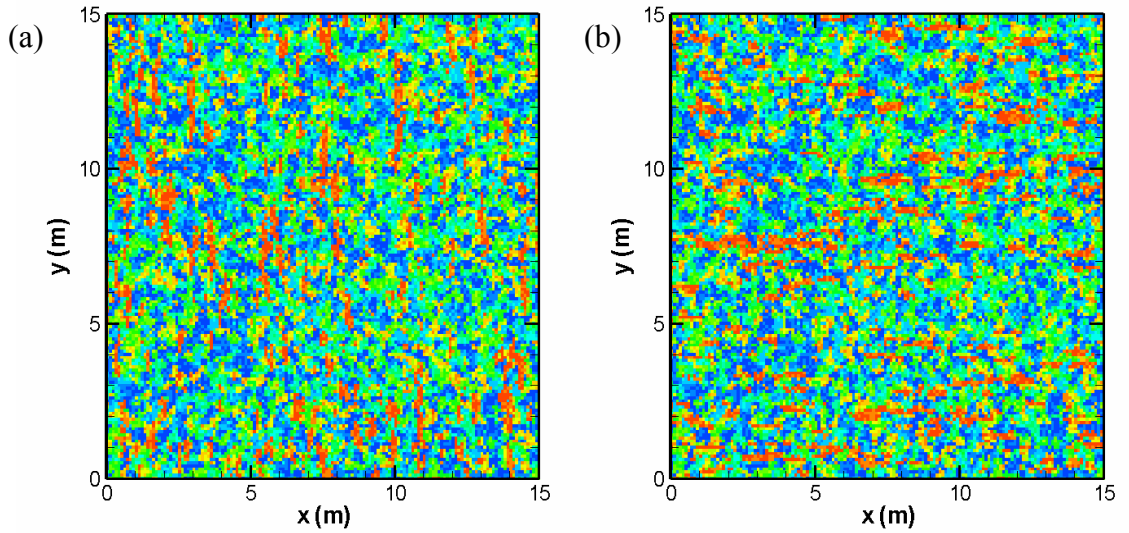

Figure 4. *Heterogeneous, anisotropic transmissivity fields generated by SISIM (red is high T, blue is low T). A 10-m long correlation length is specified for T values above the threshold and a 0.3-m long correlation length is specified for T values below the threshold. Both fields are based on the CDF shown in Figure 2.*

3.2 Accounting for fracture zone structure in the third dimension

We account for structure in the third dimension (the fracture zone thickness) by assuming that there are two sub-fractures in a ladder-like structure (Figure 1). We assume that at each (x,y) location: (1) the flow q(x,y) represents the sum of the flow in the two sub-fractures: $q_1 + q_2 = q$; (2) q, q_1 and q_2 are in the same direction; and (3) the ratio of flow between sub-fractures 1 and 2 is $\alpha = q_2/q_1$. The parameter α is denoted the fracture structure parameter. With these assumptions, straightforward algebra (Tsang and Doughty, 2002) produces the following expressions for q_1 and q_2

$$q_1 = \frac{q}{1+\alpha} \tag{1}$$

$$q_2 = \frac{q}{1+\alpha^{-1}} . \tag{2}$$

Assuming the cubic law ($q \sim b^3$) applies locally, sub-fracture apertures b_1 and b_2 may be written in terms of the apparent aperture b corresponding to q(x,y)

$$b_1 = \frac{b}{(1+\alpha)^{1/3}} \tag{3}$$

$$b_2 = \frac{b}{(1+\alpha^{-1})^{1/3}} . \tag{4}$$

For a matrix block of lateral extent $2r_m$, local fracture porosity can be defined for each sub-fracture:

$$\phi_{f1} = \frac{3b_1}{2r_m} \tag{5}$$

$$\phi_{f2} = \frac{3b_2}{2r_m} . \tag{6}$$

For each grid block, the residence time in each sub-fracture may be expressed in terms of the residence time t_w obtained from q(x,y):

$$t_{w1} = (1+\alpha)^{2/3} t_w \tag{7}$$

$$t_{w2} = (1+\alpha^{-1})^{2/3} t_w . \tag{8}$$

Two options are considered for transport through the sub-fracture network. In one case (denoted with cross-over), tracer can move freely back and forth between sub-fractures as it moves through the model of Feature A. At any given time, the probability of being in each sub-fracture is

$$P_1 = \frac{q_1}{q} = \frac{1}{1+\alpha} \tag{9}$$

$$P_2 = \frac{q_2}{q} = \frac{1}{1+\alpha^{-1}} \,. \tag{10}$$

In the other case (denoted no cross-over), each tracer particle is randomly assigned to a sub-fracture according to P_1 and P_2 when it is released into the model, and it remains in that sub-fracture until it leaves the model.

The parameter α is not readily determined by visual inspection of Figure 1, nor by laboratory measurements taken from core samples. Rather, it must be estimated based on model calibration to the STT-1b tracer test.

3.3 Transport processes

Advective transport carries tracer along with the liquid flow through the sub-fractures. On the 10-m scale of Feature A, dispersion within the fracture network arises naturally from the heterogeneous transmissivity field. Diffusion and sorption into the materials surrounding the sub-fractures are conceptualized as occurring in three matrix-block populations with different characteristic sizes: small (gouge material infilling the sub-fractures), intermediate (matrix blocks within the ladder structure), and large (the semi-infinite rock matrix outside the ladder structure). Each population has its own porosity ϕ_m, effective diffusivity D_e, and sorption strength $K_d\rho_p$.

3.4 Numerical model

The finite-difference computer code THEMMA uses Darcy's law to calculate a steady-state flow field given a two-dimensional heterogeneous transmissivity distribution and appropriate head boundary conditions. Transport is then calculated by the particle-tracking code THEMMB (Tsang and Tsang, 2001). As each particle moves along, the residence time t_w for advection through a grid block with volume V and fracture porosity ϕ_f is calculated for the two-dimensional flow field q(x,y) as

$$t_w = \phi_f \frac{V}{\frac{1}{2}\sum_i |\, q_i \,|} \tag{11}$$

where the sum i runs over all the adjacent gridblocks. Then t_w is modified to account for the fact that flow is occurring in one of two sub-fractures, using Equation (7) or (8). Finally, a time delay is added to the residence time to represent diffusion and sorption effects, based on an analytical solution. For diffusion and sorption into gouge and matrix blocks within the ladder structure, we use an analytical solution that considers flow through a three-dimensional fracture network with diffusion/sorption into finite size matrix blocks, which are approximated as spherical in shape (Rasmuson and Neretnieks, 1981). For diffusion and sorption into the matrix outside the ladder structure, we use an analytical solution that considers flow through a planar fracture with diffusion/sorption into a semi-infinite matrix (Tang et al., 1981).

For finite matrix blocks, diffusion and sorption strengths are quantified by parameters δ_0 and y (a dimensionless time) given by

$$\delta_0 = \frac{3D_e(1-\phi_f)t_w}{r_m^2\phi_f} \tag{12}$$

$$y = \frac{2D_e(t-t_w)}{K_d\rho_p r_m^2} \tag{13}$$

where D_e is the effective diffusivity, $K_d\rho_p$ is sorption strength, r_m is matrix block size, and ϕ_f and ϕ_m are fracture and matrix porosities, respectively. For a semi-infinite matrix, the controlling parameter is simply

$$\frac{(K_d\rho_p D_e)^{1/2}t_w}{(t-t_w)^{1/2}b} \tag{14}$$

where b is the fracture aperture. For both cases, for a non-sorbing tracer, $K_d\rho_p$ is replaced by ϕ_m. Effective diffusivity is defined as $D_e = D_{fw}\phi_m\tau$, where D_{fw} is free water diffusivity and τ is tortuosity. For simplicity, we write t_w instead of t_{w1} or t_{w2}, ϕ_f instead of ϕ_{f1} or ϕ_{f2}, and b instead of b_1 or b_2, but in actuality, the parameters specific to the appropriate sub-fracture must be used in Equations (12) through (14). Figure 5 illustrates Rasmuson and Neretnieks' analytical solution for a non-sorbing tracer with $\phi_m/\phi_f = 100$, and a range of δ_0 values. The solution for a semi-infinite matrix (Tang et al., 1981) is also shown. Note that diffusion increases with δ_0. For an infinite matrix, when there is little diffusion (at early times), the front is sharp; when there is more diffusion (at later times), the front is more gradual. For finite matrix blocks, when there is little diffusion (at early times), the front is sharp; when there is more diffusion (at later times), the front is more gradual; when there is much diffusion (at very late times), the matrix blocks saturate, yielding a sharp front that is delayed by a factor of ϕ_m/ϕ_f compared to the advection-only front.

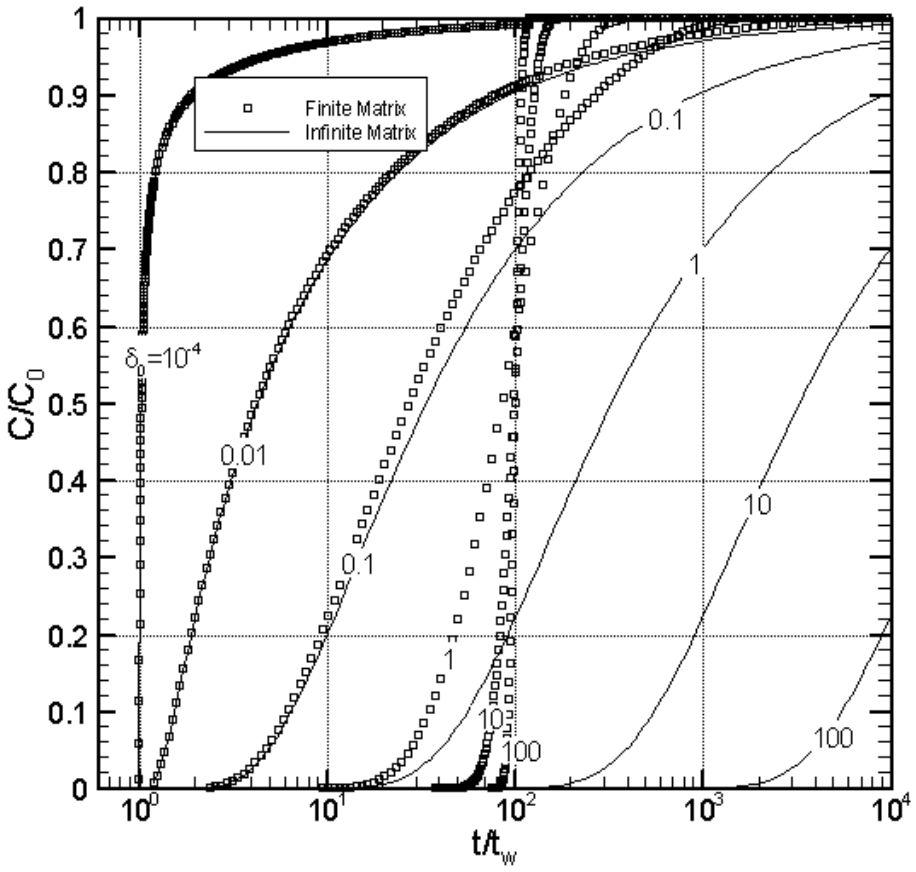

Figure 5. *Analytical solution for fracture concentration versus time for finite matrix blocks (Rasmuson and Neretnieks, 1981) and an infinite matrix (Tang et al., 1981).*

In THEMMB, after each advective time step in the fracture, a particle interacts with one of the three matrix block populations at random, according to given probabilities, as shown schematically in Figure 6. Based on Figure 1, we roughly estimate that there is a 10% probability of a particle encountering gouge, a 30% probability of encountering intermediate-size matrix blocks within the ladder structure, and a 60% probability of encountering semi-infinite matrix outside the ladder structure. These probabilities are considered adjustable parameters during calibration to the STT-1b tracer test.

Table 1 shows the δ_0 value for each of the finite-block populations for a sample problem with a non-sorbing tracer and $t_w = 10^6$ s, typical of a tracer test. Comparison with Figure 5 shows that δ_0 is large for the small and intermediate matrix blocks, indicating that diffusion into these media will significantly impact tracer transport, and that the blocks will become saturated. In contrast, for this time-scale diffusion into the semi-infinite matrix is relatively small, due to its much lower values of ϕ_m and D_e, indicating that for a non-sorbing tracer, it plays a minor role.

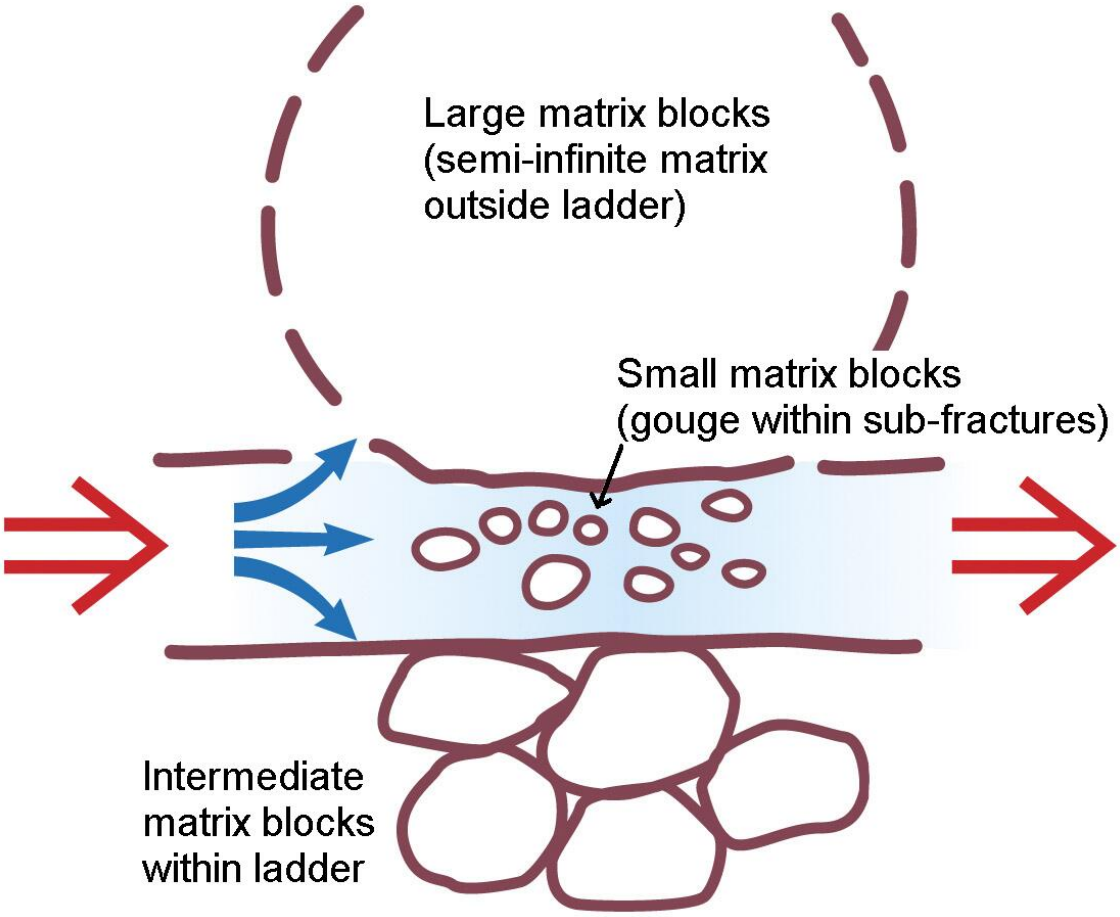

Figure 6. *Schematic representation of the three populations of matrix blocks.*

Table 1. Properties of three matrix block populations and the resulting δ_0 values for a sample problem with $\phi_f = 0.01$, $t_w = 10^6$ s, and a non-sorbing tracer (iodine).

	Small blocks Fault gouge	Intermediate blocks Altered Aspo Diorite inside ladder structure	Large blocks Unaltered Aspo Diorite outside ladder structure	Comments on how parameters were determined
r_m (m)	$5 \cdot 10^{-4}$	0.005	n/a**	Estimated from Feature A conceptual model (e.g., Figure 1)
ϕ_m	0.2	0.01	0.003	Table 2-1, Task 6A and 6B modeling task specification
D_e (m^2/s)	$2 \cdot 10^{-10}$	10^{-12}	$8.3 \cdot 10^{-14}$	Large blocks: Table 3-2, Task 6A and 6B modeling task specification
ρ_p (kg/m^3)	2700	2700	2700	Task 6A and 6B modeling task specification
δ_0	$2.4 \cdot 10^5$	12	n/a	Calculated from Eq. (12)

** The relevant parameter for diffusion and sorption into a semi-infinite medium is fracture aperture b, which we take as equal to the aperture for the intermediate matrix blocks, calculated from $3b/(2r_m) = \phi_f$.

Equation (13) shows that considering sorbing tracers has the effect of rescaling the diffusion time delay ($t-t_w$) by $K_d\rho_p/\phi_m$. Thus, if finite matrix blocks saturate, the front will be delayed by a factor $K_d\rho_p/\phi_f$ compared to the advection-only front (as opposed to the delay by ϕ_m/ϕ_f for a non-sorbing tracer). In other words, the capacity of the matrix blocks to take up tracer increases by a factor of $K_d\rho_p/\phi_m$ compared to the non-sorbing case. The parameter δ_0 does not depend directly on sorption strength, but because sorption can change the timing of transport so greatly, a value of δ_0 that produces a breakthrough curve indistinguishable from the advection-only case for a non-sorbing tracer may produce quite a different breakthrough curve for a strongly sorbing tracer. Equation (14) shows that for a semi-infinite matrix, sorbing tracers have the same effect of rescaling the diffusion time delay ($t-t_w$) by $K_d\rho_p/\phi_m$, hence they have a comparable effect in this case.

3.5 Parameters

In addition to Table 1 above, which describes matrix block parameters, Tables 2 and 3 summarize general parameters of the model and tracer properties, respectively.

Table 2. Model dimensions, transmissivity field properties, flow field properties, and particle-tracking specifications.

Parameter	Value	Comments
nx, ny, nz (number of grid blocks)	150, 150, 1	Want adequate resolution of heterogeneous T(x,y) field
dx, dy, dz (grid spacing)	0.10 m, 0.10 m, 0.02 m	dx, dy are lesser of 15-m model extent divided by nx, ny and minimum spatial correlation length; dz from Feature A conceptual model
Sequential indicator simulation using a CDF for $\log_{10}$T based on 15 well-test analyses for 5 boreholes*		Flexible means of producing realistic looking heterogeneous T fields
Mean, standard deviation $\log_{10}$ T	-7.5*, 0.58* (T in m^2/s)	Output of SISIM
Spherical variogram range – thresholds 1-4	0.3 m	Estimated from Feature A conceptual model
Spherical variogram range – threshold 5	1 m	Estimated from Feature A conceptual model
Fracture porosity	0.0017*	From the cubic law, mean T, and dz
Head gradient	0.001 m/m	Task 6B2 specification
Injection period	10^7 years	Task 6B2 specification
Particle release location	x = 6.5 to 8.5 m, y = 5 m	Task 6B2 specification
Number of particles	100,000 to 500,000	Need enough particles to resolve features of breakthrough curves
Particle collection location	y = 15 m	Task 6B2 specification

*initial model value; varied during STT-1b calibration

Table 3a. Tracer properties for small matrix blocks (gouge).

Tracer	***Matrix sorption coefficient*** K_d (m^3/kg)	***Effective matrix diffusivity*** D_e (m^2/s)	Comments K_d all same as unaltered diorite D_e all taken from $D_{fw}\tau = 10^{-9}$
I	0	$2 \cdot 10^{-10}$	
Sr	$4.7 \cdot 10^{-6}$*	$2 \cdot 10^{-10}$	
Co	$8 \cdot 10^{-4}$*	$2 \cdot 10^{-10}$	
Tc	0.2*	$2 \cdot 10^{-10}$	
Am	0.5*	$2 \cdot 10^{-10}$	

*initial model value; varied during STT-1b calibration

Table 3b. Tracer properties for intermediate matrix blocks (altered diorite).

Tracer	***Matrix sorption coefficient*** K_d (m^3/kg)	Effective matrix diffusivity D_e (m^2/s)	Comments K_d all same as unaltered diorite D_e all taken from $D_{fw}\tau = 10^{-10}$
I	0	10^{-12}	
Sr	$4.7 \cdot 10^{-6}$	10^{-12}	
Co	$8 \cdot 10^{-4}$	10^{-12}	
Tc	0.2	10^{-12}	
Am	0.5	10^{-12}	

Table 3c. Tracer properties for semi-infinite matrix (unaltered diorite outside Feature A ladder-like structure).

Tracer	***Matrix sorption coefficient*** K_d (m^3/kg)	***Effective matrix diffusivity*** D_e (m^2/s)	Comments
I	0	$8.3 \cdot 10^{-14}$	Table 3-2, Task 6A and 6b modeling task specification
Sr	$4.7 \cdot 10^{-6}$	$4 \cdot 10^{-14}$	Table 6-11, Task 6A and 6b modeling task specification
Co	$8 \cdot 10^{-4}$	$2.9 \cdot 10^{-14}$	Table 3-2, Task 6A and 6b modeling task specification
Tc	0.2	$4 \cdot 10^{-14}$	Table 3-2, Task 6A and 6b modeling task specification
Am	0.5	$4 \cdot 10^{-14}$	Table 3-2, Task 6A and 6b modeling task specification

4 Results - Performance measures

4.1 Task 6A

4.1.1 Model representation of STT-1B conditions

A non-uniform initial head distribution was identified in Feature A prior to test STT-1b. If these heads are assumed to represent steady-state conditions, then head boundary conditions for Feature A must be non-uniform as well. However, the range of variation of the observed head distribution (~1 m) is much smaller than the observed drawdown during the test (~5 to ~15 m), so the flow field is probably not much affected by the non-uniform boundary. Therefore, we assume uniform constant-head boundary conditions for Feature A. Although the lateral extent of the Feature A model is nominally 15 m by 15 m (see Table 2), a coarse grid is added on all sides of this region to enable constant head boundaries to be applied about 50 m away, to minimize distortion of the flow field. Constant rates of 41.9 mL/hr injection in borehole KXTT1 R2 and 0.401 L/min pumping in borehole KXTT3 R2 are specified for the STT-1b tracer test. However, the observed drawdowns show irregular changes that imply other head or flow conditions in the vicinity of Feature A were changing during test STT-1b. This unknown variation is not included in the model.

Figure 7 shows the model representation of the HTO input concentration. Similar representations are used for I, Sr, and Co, whereas Tc and Am use a constant injection rate for 4 hours. When examining the details of breakthrough curves on log-log scales, it is imperative that the entire injection history be modeled, not just the primary 4-hour pulse. Tracer is released over an area composed of 3 by 3 adjacent grid cells (0.3 by 0.3 m).

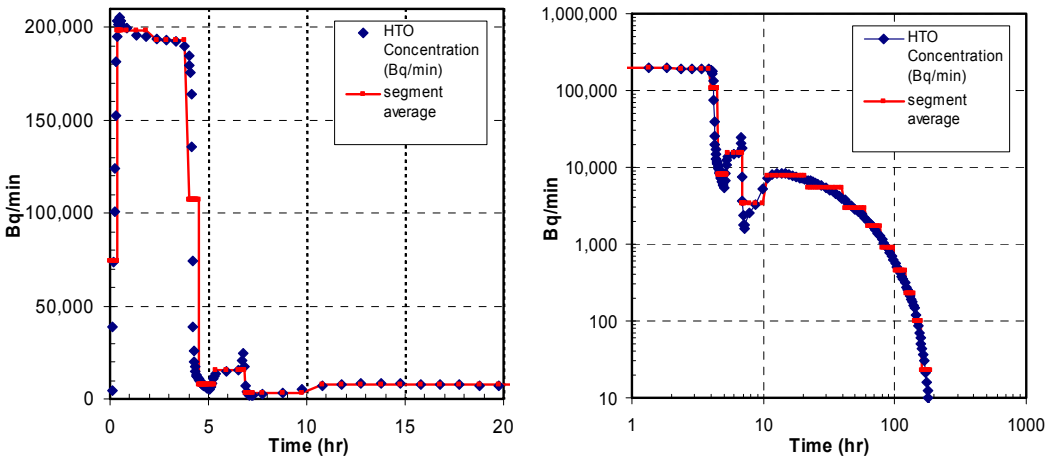

Figure 7. *Injection concentration for HTO during the STT-1b tracer test. The linear scale on the left emphasizes the main portion of the input – a 4-hour pulse. The log-log scale on the right emphasizes the long tail, which cannot be ignored if log-log comparisons of tracer breakthrough curves are to be made.*

Figure 8 compares the observed HTO breakthrough curve and that calculated with the initial model. Overall, the agreement is not very good. The model peak is much too early, somewhat too high, and the tail shows a sharp drop shortly after the main 4-hour injection pulse ends whereas the observed data shows a much more gradual decline. The late-time tail (beyond about 40 hours) is modeled adequately.

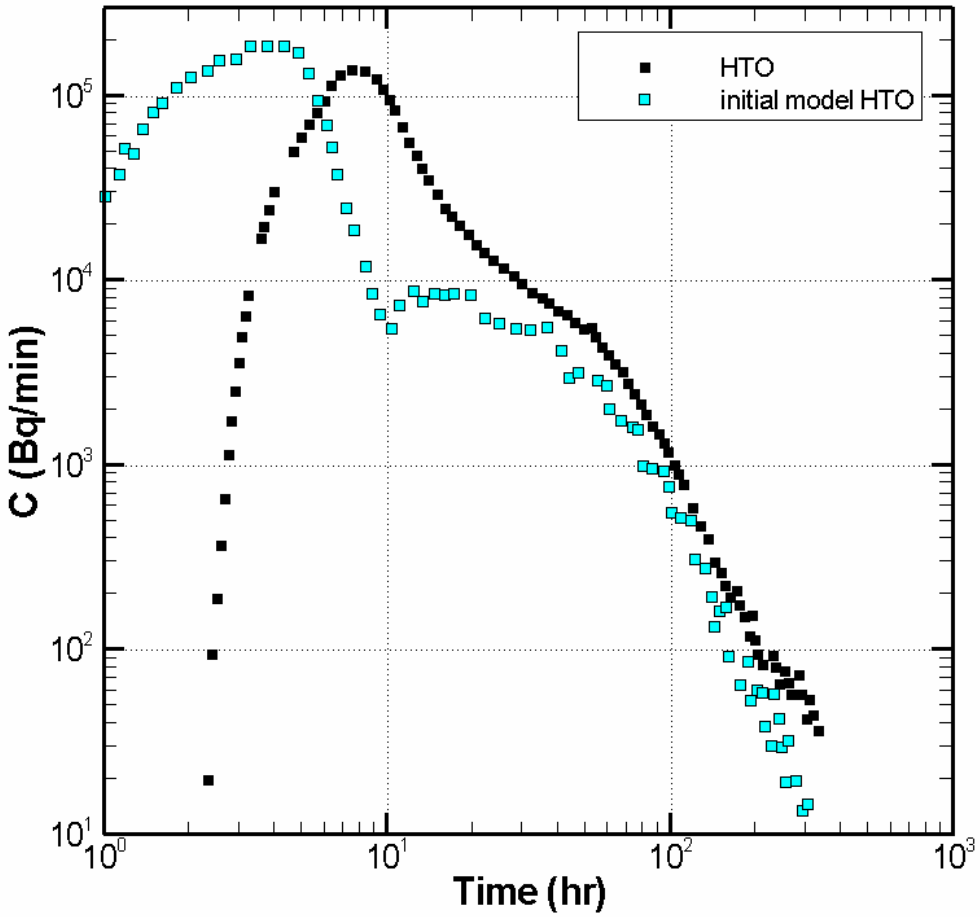

Figure 8. *STT-1b HTO breakthrough curve for the initial model (model parameters are given in Tables 1- 4).*

4.1.2 Model calibration

The observed drawdowns and tracer breakthrough curves obtained during tracer test STT-1b are used for model calibration. Parameters that are not considered to be well-constrained from available field data are varied during the calibration process: the mean value of the transmissivity, the variability of the transmissivity field, the fracture porosity ϕ_f, the relative proportion of different matrix block populations, the value of the fracture structure parameter α, and the soprtion strength K_d of the gouge for the various tracers. Table 4 summarizes the range of parameters considered.

Table 4. Parameters varied during model calibration to tracer test STT-1b.

Parameter	Initial model	Range considered	Data used for calibration	Calibrated model
Mean T (m^2/s)	3.5E-8	3.5E-8 – 3.5E-7	Drawdowns	3.5E-7
T field heterogeneity (σ_{log10T})	0.58	0 – 2.17	HTO BTC	1.38
Fracture porosity ϕ_f	0.0017	0.0017 – 0.0425	HTO BTC	0.011
Relative proportion of different matrix block populations	10/30/60 (gouge%/ intermediate%/ large%)	5/30/65 – 25/30/45	HTO BTC	25/30/45
Fracture structure parameter α (no cross-over)	0.01	0 to 1	HTO BTC	0.03
Gouge K_d (m^3/kg)				
Strontium	4.7E-6	4.7E-6 – 3E-4	Sr BTC	1.5E-4
Cobalt	8E-4	8E-4 – 8E-3	Co BTC	4E-3
Technitium	0.2	0.2 – 2	Tc non-arriaval	1
Americium	0.5	0.5 – 5	None	2.5

Mean transmissivity

Table 5 shows the drawdowns observed at the five borehole intervals in Feature A, along with those calculated with the original model, which has a mean $\log_{10}T$ value of -7.45 (T = 3.5E-8 m^2/s). The modeled drawdowns are much too large. Recall that the model mean $\log_{10}T$ value came from the CDF shown in Figure 2, which was developed based on transmissivity values inferred from various Feature A hydraulic tests (Winberg et al., 2000). Apparently, there is an inconsistency between those results and the drawdowns observed during the STT-1b tracer test. Increasing all the T values in the model by a factor of 10 produces drawdowns that are much more in line with the observed ones, as shown in Table 5. The new model has the same standard deviation and spatial correlation structure as the original model, but has a mean $\log_{10}T$ value of -6.45 (T = 3.5E-7 m^2/s). Drawdowns for another stochastic realization of the new model are also shown in Table 5, to illustrate the kind of model variability to be expected from changes in the details of the T distribution.

Table 5. Observed and modeled drawdowns during tracer test STT-1b.

Borehole	Observed drawdown (m)	Original model drawdown (m) (mean T=3.5E-8 m^2/s)	New model drawdown (m) (mean T=3.5E-7 m^2/s)	
			Realization 1	Realization 2
KXXT3	-15.0	-265	-9.4	-9.1
KXTT1	-5.1	-94	-2.7	-3.2
KXTT4	-4.1	-120	-3.3	-4.2
KXTT2	-12.4	-82	-2.6	-2.8
KA3005A	-4.6	-72	-1.9	-2.5

Note in Table 5 that the observed drawdown in borehole KXTT2 is much larger than that in the other three observation boreholes, despite the fact that they are similar distances from the pumping borehole KXXT3, suggesting strong heterogeneity in the Feature A transmissivity distribution. Such heterogeneity makes analysis of hydraulic tests difficult, and the use of analytical solutions that assume homogeneous media unreliable. Therefore, we feel justified using larger transmissivities than those shown in Figure 2, which are obtained from such analytical solutions.

It should be pointed out that the value of the mean transmissivity does not affect tracer breakthrough curves at all for Tasks 6A and 6B, in which well injection and production rates determine the flow field. For Task 6B2, in which a regional head gradient is specified, fluid flow velocity is proportional to mean transmissivity, so tracer arrival times do depend on the choice of mean transmissivity. We expect that arrival time will depend inversely on mean transmissivity for the advection-only case, and as diffusion and sorption become more important, the longer travel time accompanying lower transmissivity will enhance the opportunity for diffusion and sorption, further delaying tracer arrival.

T field heterogeneity

It is unlikely that the full variability of the T field is sampled by the few well-test available for Feature A (tests at only five locations). Preliminary sensitivity studies using T fields with different amounts of heterogeneity (e.g., Figures 3a and 3b) have indicated that the leading edge of the breakthrough curve (the first-arrival time of tracer) does not depend very much on how heterogeneous the transmissivity field is, but the overall shape of the breakthrough curve does. As heterogeneity increases, it takes longer for all the particles to reach the model outlet, resulting in more gradual breakthrough curves, which Figure 8 show that the initial model of the STT-1b tracer test requires. Therefore, the greater variability of the T field shown in Figure 3b is used to represent Feature A.

Fracture porosity □f

Note that ϕ_f is the fraction of void space within the complex fracture zone, not within the fractured rock block as a whole. For the complicated structure of Feature A, the use of the cubic law to determine fracture porosity ϕ_f from transmissivity is not considered reliable, so ϕ_f is considered a model parameter that can be adjusted. Figure 9 shows the results of a sensitivity study in which the fracture porosity ϕ_f is varied. Larger values of ϕ_f delay the arrival of the peak, which the initial model of the STT-1b tracer test requires. It turns out that $\phi_f = 0.011$, the value obtained with the cubic law for the higher mean transmissivity of 3.5E-7 m^2/s, provides a reasonble match to the observed peak time for HTO,

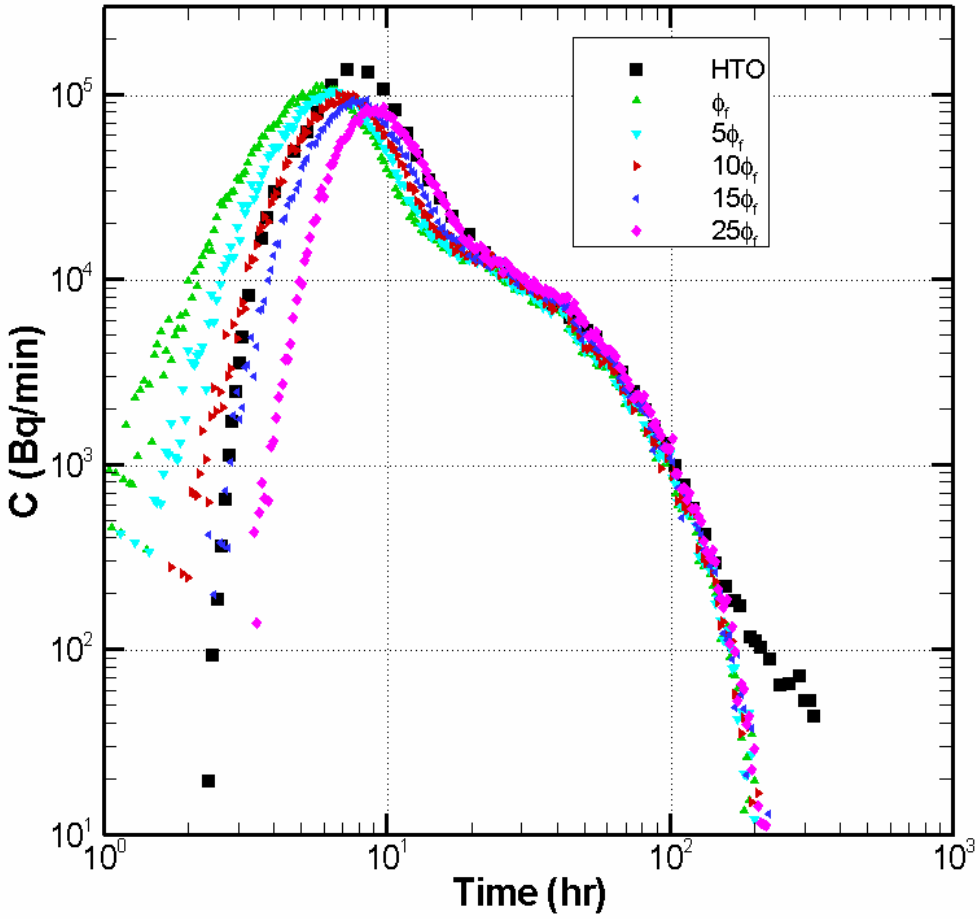

Figure 9. *STT-1b HTO breakthrough curves for various values of fracture porosity ϕ_f. For this sensitivity study, the base $\phi_f = 0.0017$.*

Relative proportion of different matrix block populations

The relative proportion of different matrix block populations is quite uncertain, but it has a stong effect on the breakthrough curves. For the tracer test, the percentage of gouge present is the most important factor. Sensitivity studies (Figure 10) indicate that increasing the gouge percentage from the initial value of 10% to 25% helps in matching

the HTO breakthrough curve. In this sensitivity study the percentage of intermediate blocks is maintained at 30%, so the percentage of semi-infinite matrix varies as the gouge percentage varies. However, for non-sorbing tracers the breakthrough curves are not sensitive to the relative percentages of intermediate blocks and semi-infinite matrix.

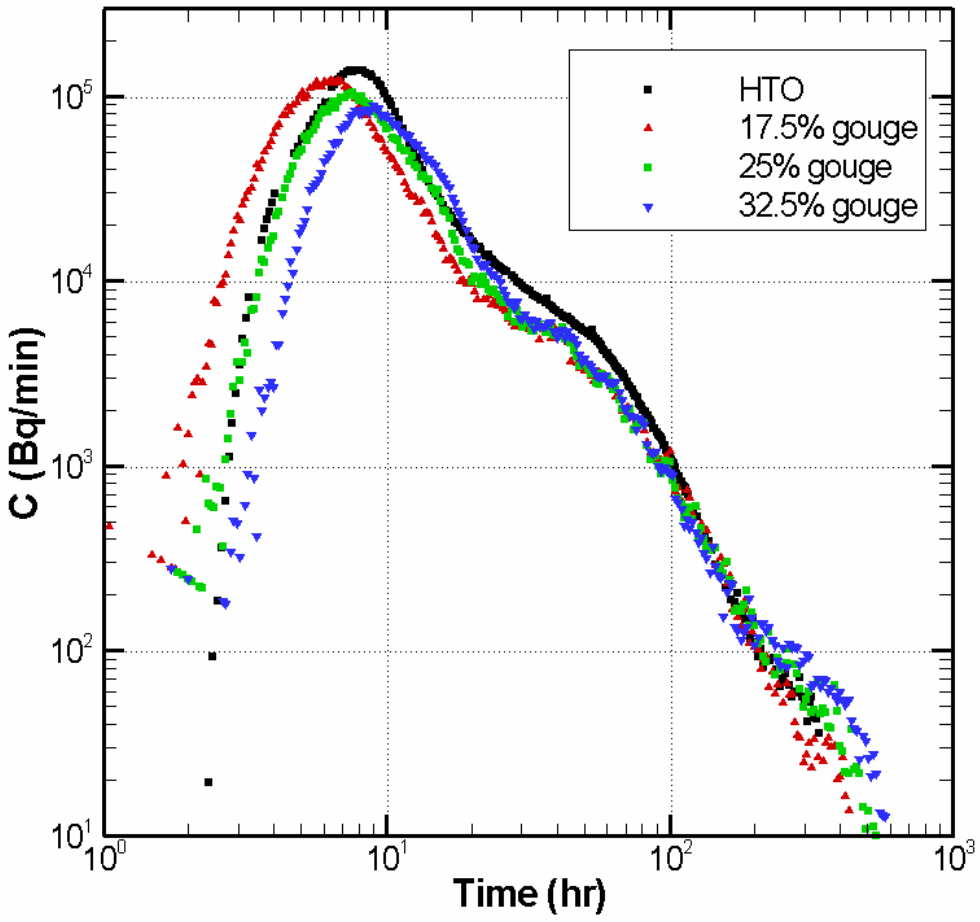

Figure 10. *STT-1b HTO breakthrough curves for various percentages of gouge.*

Fracture structure parameter

We have no a priori knowledge of the value of the fracture structure parameter, so it is varied over its entire range from 0 to 1 during calibration. Figure 11 shows a sensitivity study in which α ranges from 0.01 to 1. Increasing α delays the arrival of the peak and lowers its height somewhat, but the main effect is on the tail. For small values of α, a very small, very late second peak is visible, representing a small amount of flow through the smaller sub-fracture. As α grows, the second peak becomes bigger and arrives earlier, until it merges with the first peak, producing the gradually decreasing tail observed in the field data. Values of α of 0.03 and 0.2 each improve the model in one specific range of times: $\alpha = 0.03$ provides an improved match to the final tracer arrivals, wherease $\alpha = 0.2$ improves the match just after the peak.

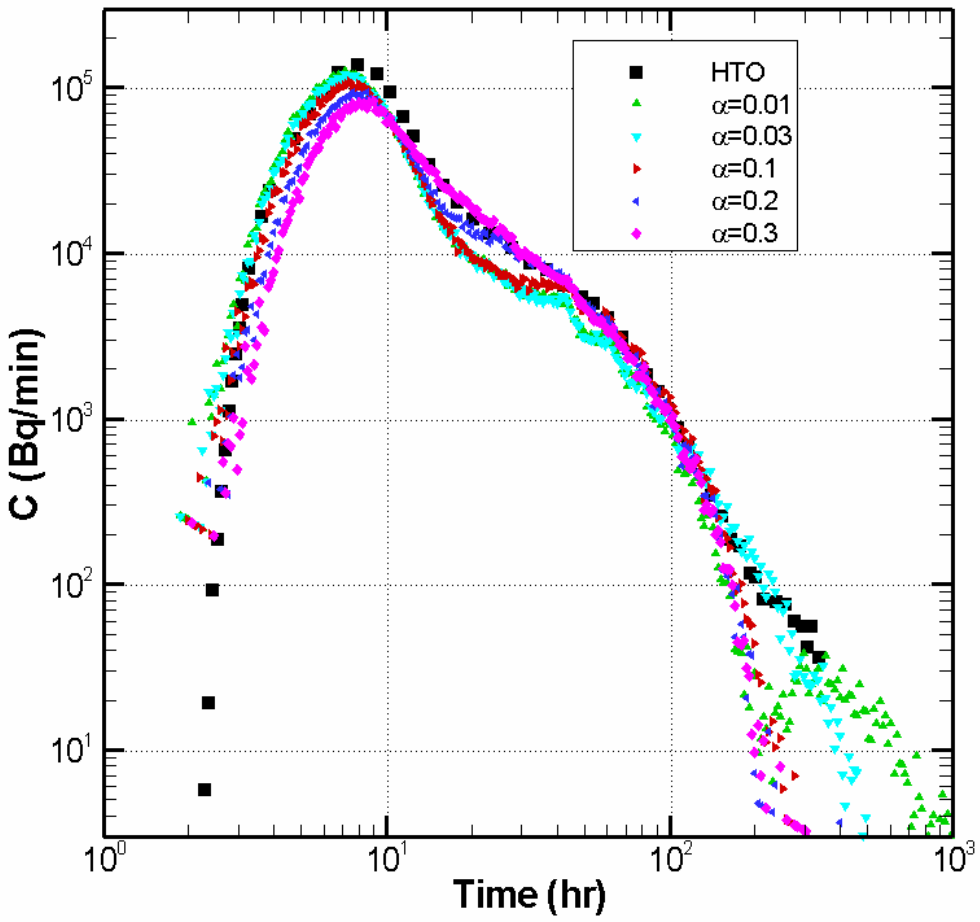

Figure 11. *STT-1b HTO breakthrough curves for various values of α.*

Figure 12 shows the breakthrough curves for HTO and iodine (I) using the calibrated parameters shown in the far right column of Table 4. Note that the observed iodine data was not used during the calibration process.

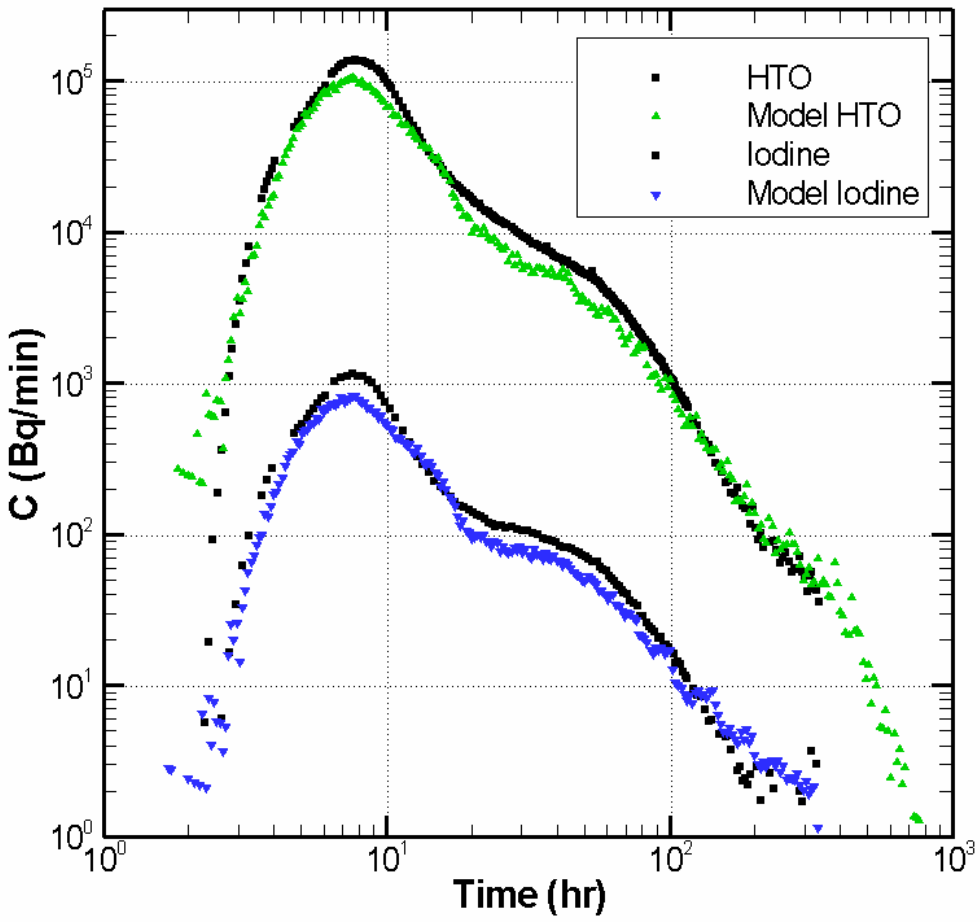

Figure 12. *STT-1b HTO and I breakthrough curves for the calibrated model.*

Gouge sorption strength Kd

The sorption strengths K_d given in Table 3 are all based on unaltered diorite, which is considered appropriate for the semi-infinite matrix. In the absence of other information it may also be adequate for the intermediate matrix blocks (dimension 1 cm). For the gouge (dimension 1 mm), a better source of information may be the K_d values obtained from tests on crushed material (Task 6A and 6B modeling task specification, Table 6-12). We consider the source of the gouge to be a mixture of altered and unaltered diorite, so the K_d values for these two materials are averaged for Sr and Cs (a surrogate for Co). This yields approximately an order of magnitude increase in K_d, which is also assigned to Tc and Am, for which crushed K_d data are lacking. This provides the starting point for our calibration study. Figure 13 shows the STT-1b breakthrough curves for Sr using a range of gouge K_d values. The match is much improved for K_d = 1.5E-4 m^3/kg, and is considered adequate.

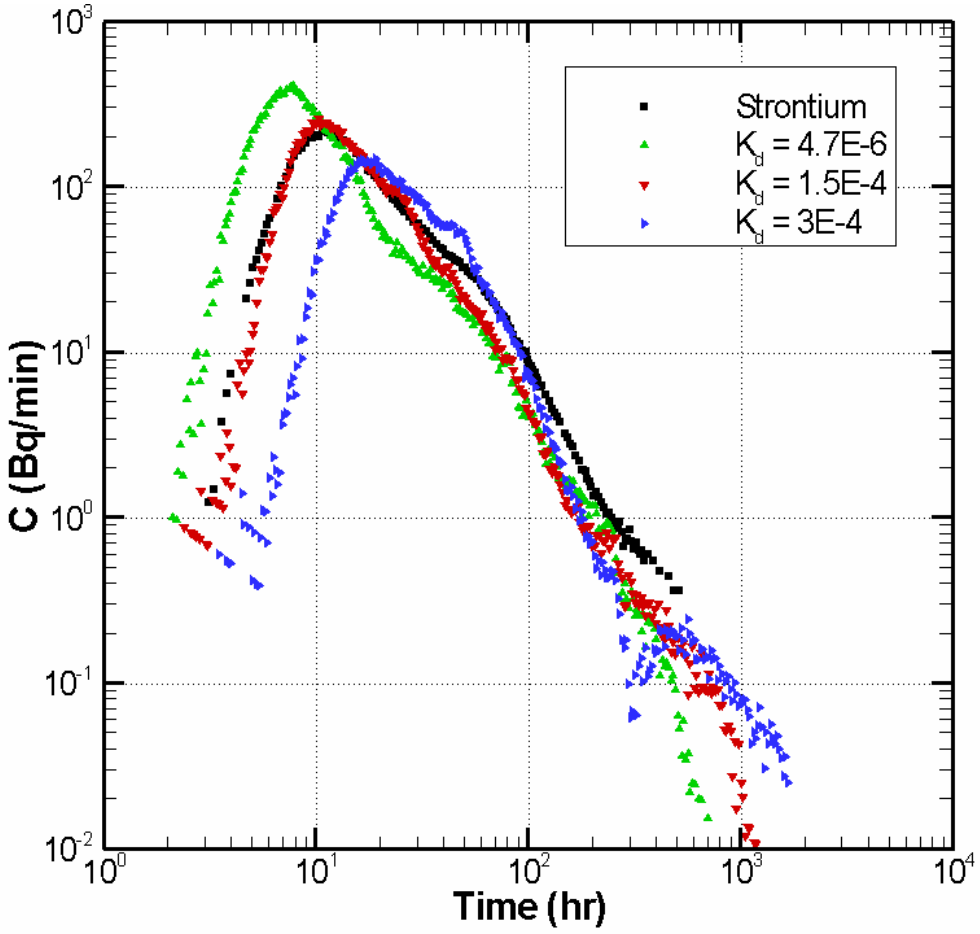

Figure 13. *STT-1b Sr breakthrough curves for various values of gouge K_d.*

Figure 14 shows the Co breakthrough curves for various values of gouge K_d. The Co match is slightly improved for K_d = 3.7E-3 m^3/kg, with about the right timing, but the model peak is the wrong overall shape and is too high. A better breakthrough curve match can be obtained for Co by varying the K_d values for all matrix blocks. However, varying K_d values for intermediate matrix blocks and semi-infinite matrix is not justified based on physical grounds, so the resulting K_d values are not used for PA studies.

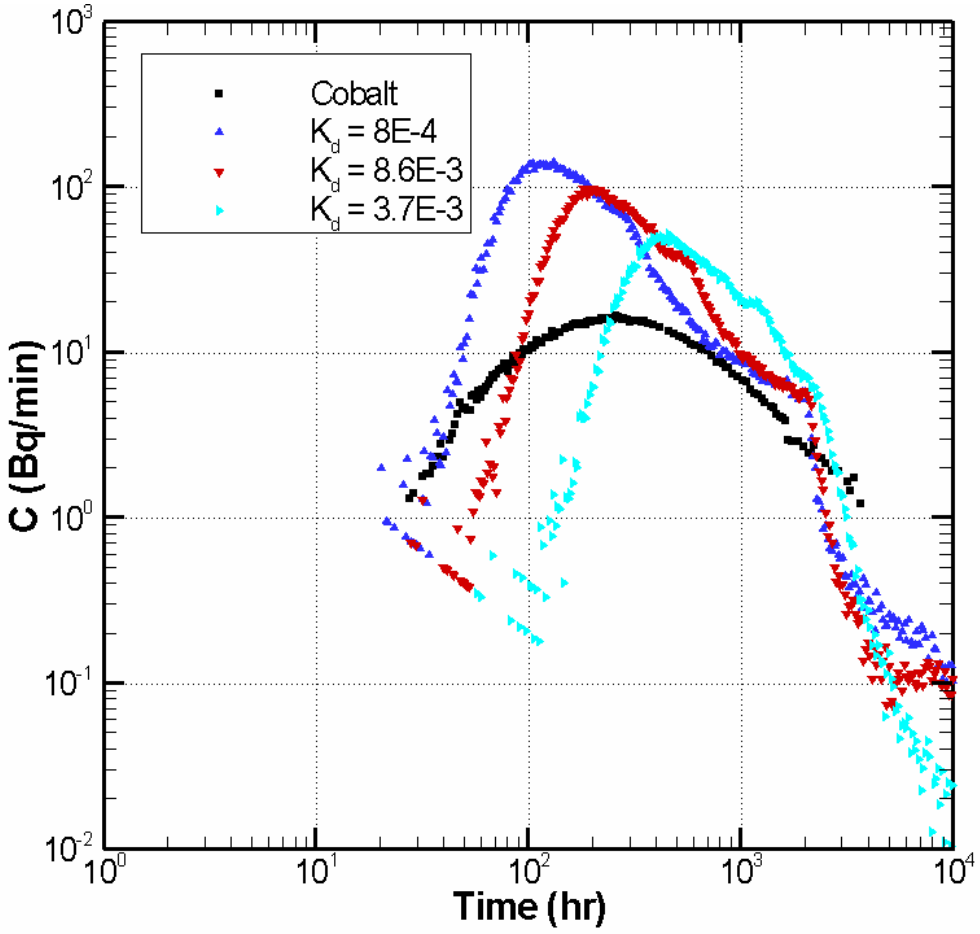

Figure 14. *STT-1b Co breakthrough curves for various values of gouge K_d.*

Figure 15 shows the modeled breakthrough curves for Tc and Am for the original K_d values and for K_d values increased by a factor of five, the same increase factor used for the Co match. The Tc peak is probably too late and too small to be detectable in the field, consistent with the non-detect of Tc. Figure 16 summarizes all the breakthrough curves for the calibrated model.

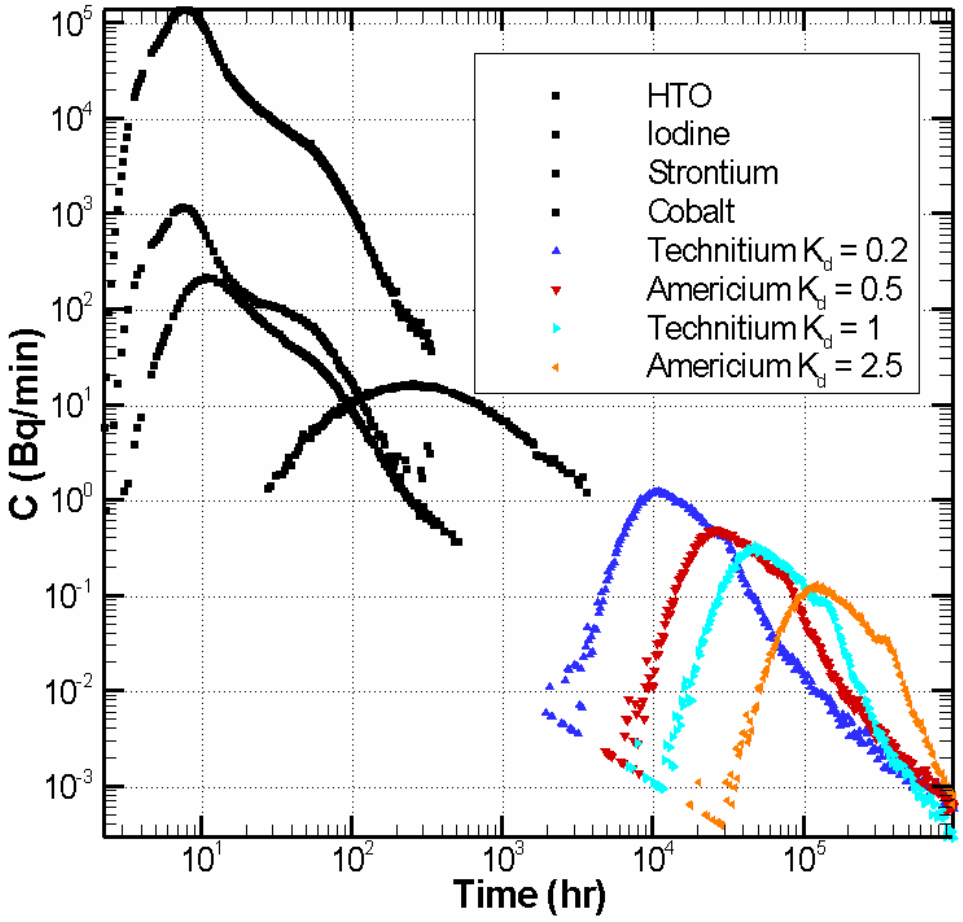

Figure 15. *STT-1b breakthrough curves for all tracers and modeled breakthrough curves for Tc and Am.*

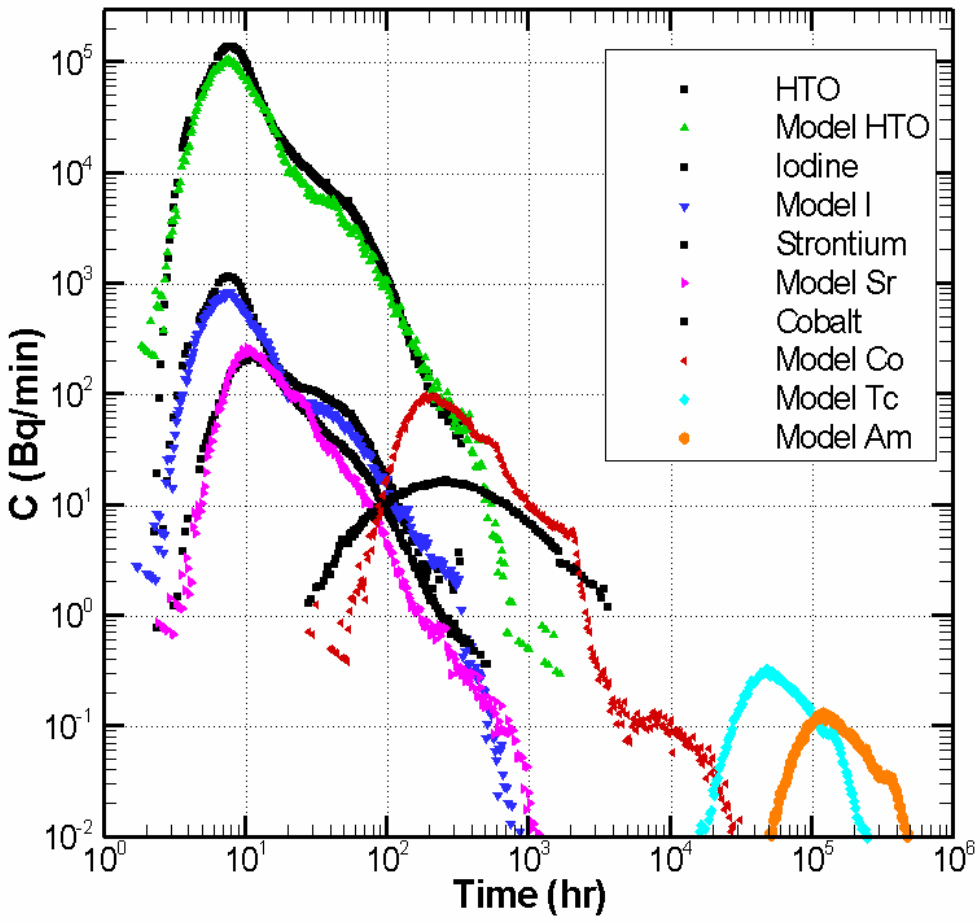

Figure 16. *Summary of STT-1b breakthrough curves for the calibrated model.*

4.2 Task 6B

PA timing is obtained by reducing the production and injection rates of the STT-1b tracer test by a factor of 1000. Both constant-injection-rate and pulse-injection transport problems are analyzed. In each case the particle tracker releases a total of 200,000 particles. The five tracers used are I (non-sorbing), Sr (slightly sorbing), Co (moderately sorbing), and Tc and Am (strongly sorbing). The results shown in this section use the calibrated model parameters shown in the far right column of Table 4.

Figure 17 shows the time history of tracer arrival at the production well for the constant injection case, for each of the tracers and for an advection-only case in which there are no matrix blocks at all. The spread among arrival times for the various tracers is enormous, indicating that sorption can greatly delay transport. The delay between the advection-only arrival curve and the curve for I indicates that diffusion itself is significant, because this tracer is essentially non-sorbing.

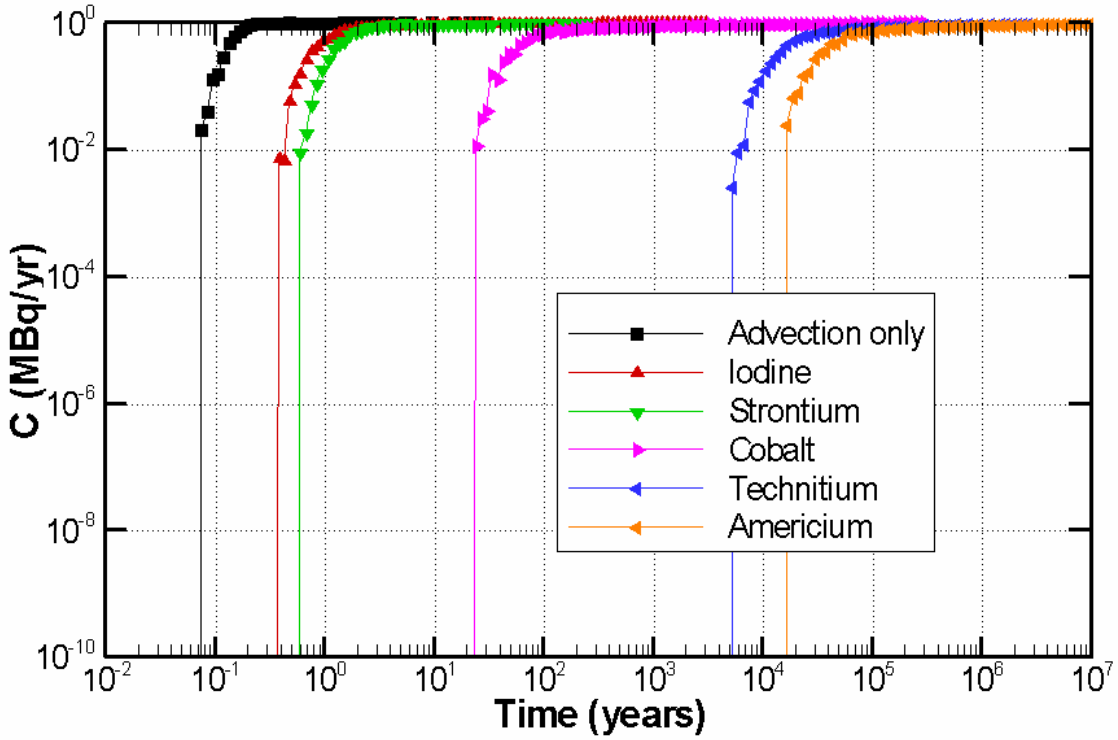

Figure 17. *Time history of tracer arrival at borehole KXTT3 for Task 6B, constant tracer injection.*

Figure 18 shows the time history of tracer arrival at the production well for the pulse injection case, for each of the tracers and for an advection-only case in which there are no matrix blocks at all. The decrease in peak height as sorption increases is a natural consequence of the increase in peak width (note that time is plotted on a log scale). For the advection-only case, the lack of diffusion and sorption makes the fronts sharp enough for two individual arrival pulses, corresponding to flow through the two sub-fractures, to be seen. For all the tracers, diffusion and sorption into the semi-infinite matrix produces more gradual fronts, which causes the two sub-fracture pulses to merge together, creating a long tail. Table 6 summarizes the recovery times for 5%, 50%, and 95% of the Dirac pulse. Table 7 shows the maximum release rates for the Dirac pulse calculations; the peak values are simply read off the modeled arrival history shown in Figure 18.

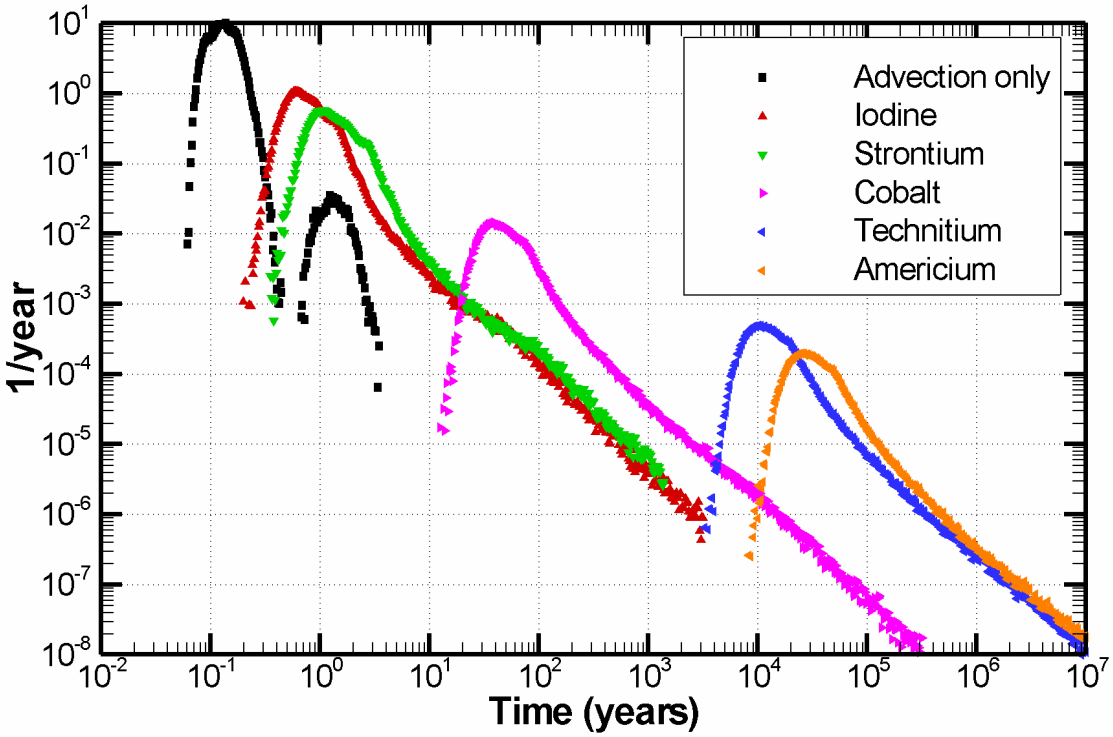

Figure 18. *Time history of tracer arrival at borehole KXTT3 for Task 6B, pulse tracer injection.*

Table 6. Time (years) for recovery of 5, 50, and 95% of the Dirac pulse injection for Task 6B.

Tracer	5%	50%	95%
Advection-only	0.0883	0.140	0.243
I	0.463	0.968	29.9
Sr	0.787	1.76	58.3
Co	28.7	67.0	5700
Tc	7690	1.89E4	1.84E6
Am	1.93E4	4.74E4	4.53E6

Table 7. Maximum release rate (1/year) for Dirac pulse injection for Task 6B.

Advection-only	I	Sr	Co	Tc	Am
10	1.1	0.57	0.014	5.0E-4	2.0E-4

4.3 Task 6B2

A steady-state flow field through the 15 m x 15 m model of Feature A is obtained by imposing a head gradient of 0.001 between the top and bottom model boundaries, while keeping the side boundaries closed (e.g., see Figure 3b). The transport problem considers a 2 m long line source of tracer, located 5 m from the upgradient model boundary, and oriented perpendicular to the nominal flow direction defined by the constant-head boundaries. An aggregate tracer arrival time history is calculated for the entire 15 m extent of the top model boundary.

Both constant-injection-rate and pulse-injection transport problems are analyzed. In each case the particle tracker releases a total of 200,000 particles. The five tracers used are I (non-sorbing), Sr (slightly sorbing), Co (moderately sorbing), and Tc and Am (strongly sorbing). The results shown in this section use the calibrated model parameters shown in the far right column of Table 4.

Figure 19 shows the calculated time history of tracer arrival at the down-gradient model boundary for the constant injection case, for each of the tracers as well as for an advection-only case in which there are no matrix blocks at all. Arrivals are slightly earlier than for Task 6B, but the relative differences between the different tracers are the same.

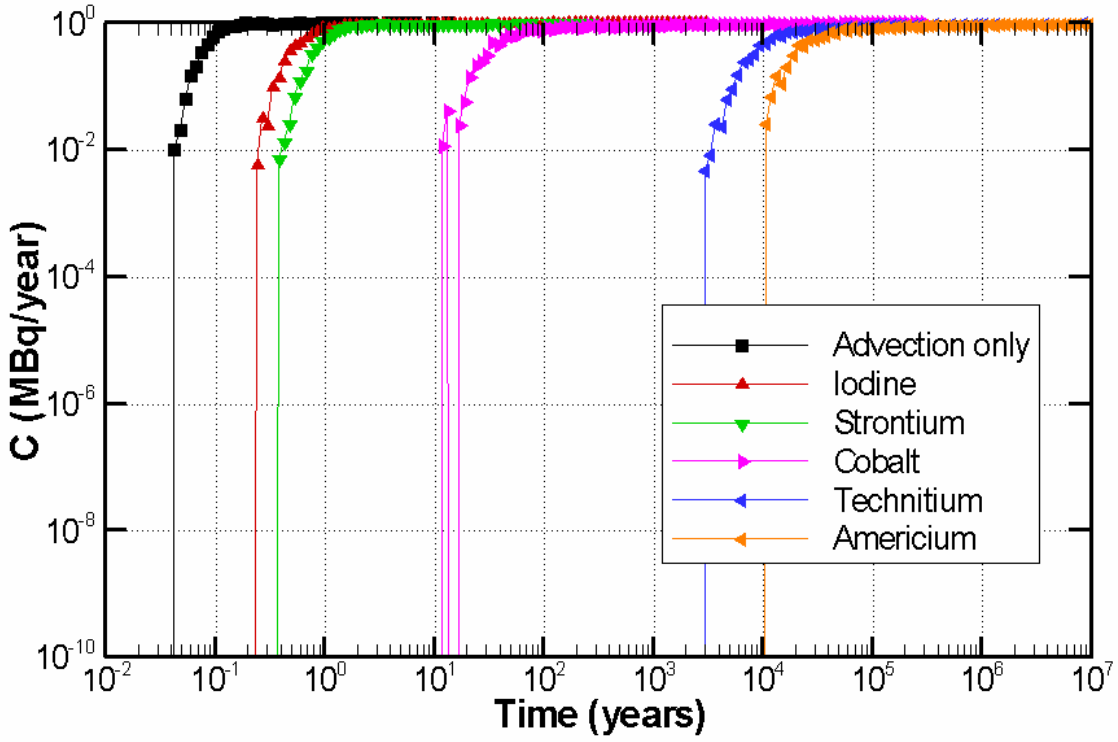

Figure 19. *Time history of tracer arrival at down-gradient model boundary for Task 6B2, constant injection.*

Figure 20 shows the calculated arrival curves with a pulse injection of tracer. The same dependence on sorption strength as seen for the constant-injection-rate case is apparent. Table 8 summarizes the recovery times for 5%, 50%, and 95% of the Dirac pulse. Table 9 shows the maximum release rates for the Dirac pulse calculations; the peak values are simply read off the modeled tracer arrival history shown in Figure 20.

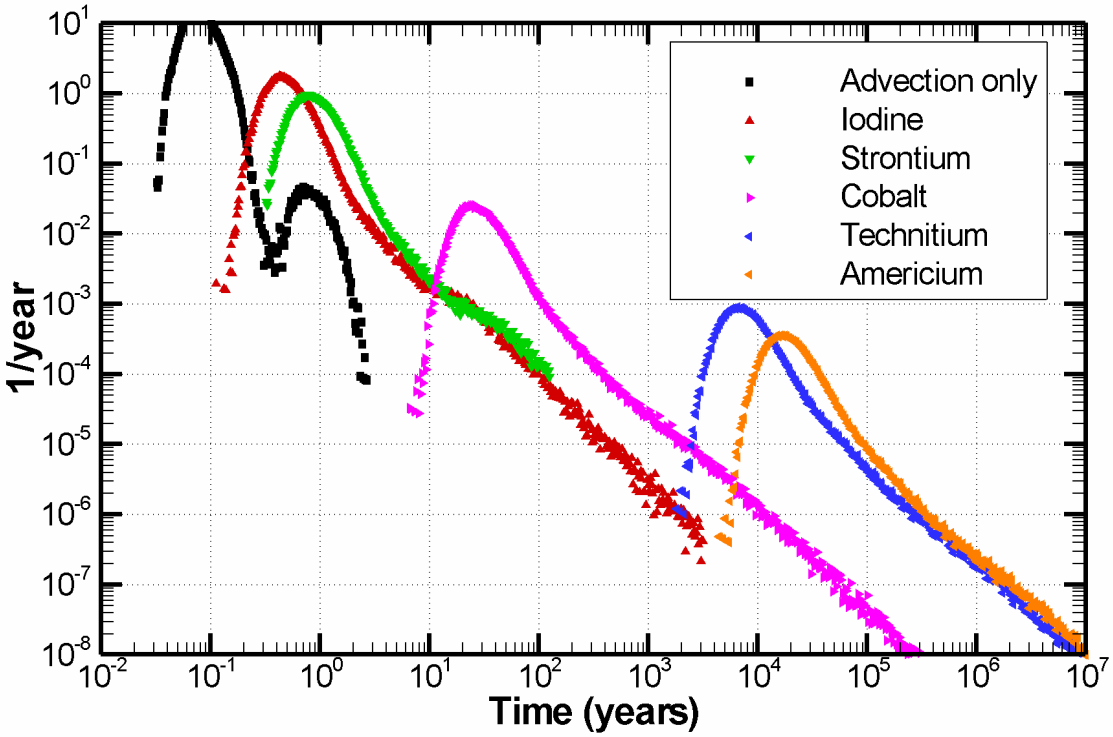

Figure 20. *Time history of tracer arrival at down-gradient model boundary for Task 6B2, pulse injection.*

Table 8. Time (years) for recovery of 5, 50, and 95% of the Dirac pulse injection for Task 6B2.

Tracer	5%	50%	95%
Advection-only	0.0532	0.0882	0.180
I	0.299	0.597	14.3
Sr	0.532	1.09	28.6
Co	17.2	38.5	2,550
Tc	4.63E3	1.06E4	8.24E5
Am	1.16E4	2.60E4	2.02E6

Table 9. Maximum release rate (1/year) for Dirac pulse injection for Task 6B2.

Advection-only	I	Sr	Co	Tc	Am
14.5	1.8	0.96	0.025	9.2E-4	3.6E-4

4.4 Sensitivity studies

In addition to the sensitivity studies shown in Section 4.1 as part of the STT-1b tracer test calibration, here we show two sensitivity studies based on PA timing. The first examines the effect of allowing cross-over between sub-fractures. The second examines the effect of fracture structure parameter α for an advection-only case (no diffusion or sorption at all), for a non-sorbing tracer, and for a strongly sorbing tracer. In both studies, the influence of the semi-infinite matrix is minimized by using a low effective diffusivity for this type of matrix diffusion, thus yielding relatively sharp tracer arrival curves (compare Figure 5).

4.4.1 The effect of cross-over

Figure 21 compares modeled breakthrough curves for cases with and without cross-over between sub-fractures. A case with α=0 is also shown for reference. It is apparent that the no-cross over case accentuates the effect of the sub-fractures, with distinct humps in the breakthrough curves representing arrival in each sub-fracture. When cross-over can occur freely (i.e., a new sub-fracture is picked at random every time step), the effect of the individual sub-fractures tend to average out. The no-cross-over and free-cross-over cases may be considered to be limiting cases of a range of cross-over options. The most geologically realistic case might be to allow cross-over with some probability each time step.

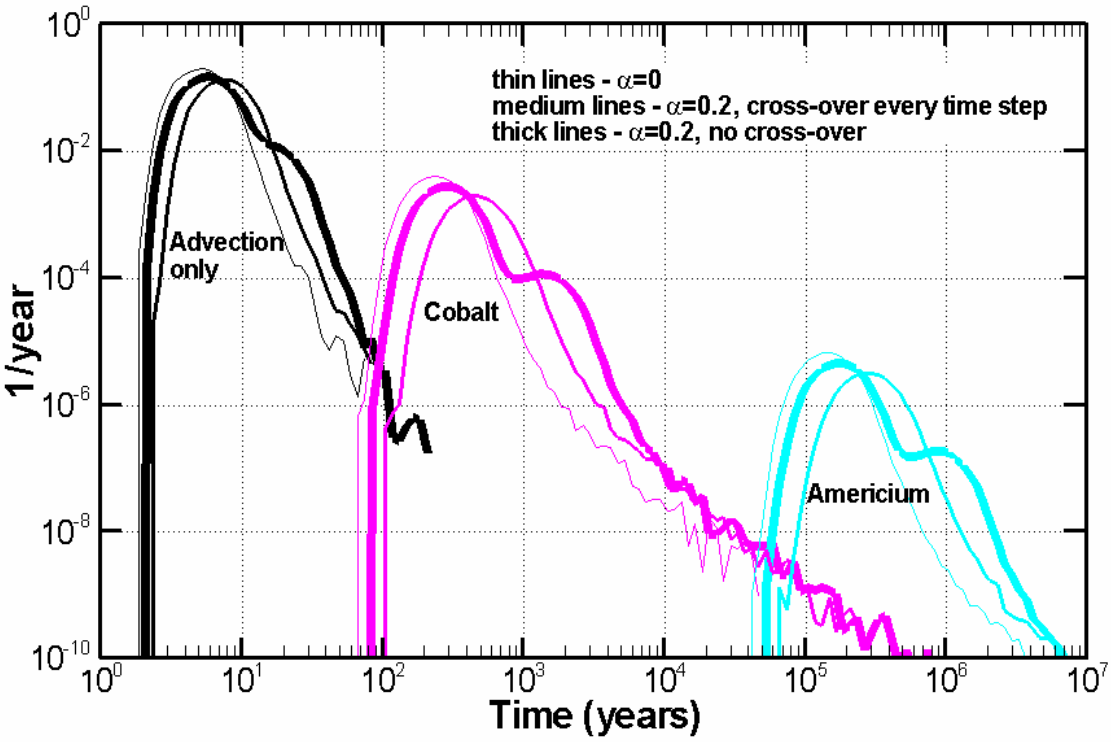

Figure 21. *The effect of cross-over for an advection-only case, a moderately sorbing tracer (Co) and a strongly sorbing tracer (Am). An α=0 breakthrough curve is also shown for comparison in each case.*

4.4.2 Fracture structure parameter $\alpha=q_2/q_1$

The fracture structure parameter $\alpha=q_2/q_1$ is varied over the range 1, 0.1, 0.01, 0.001, and 0. Figure 22 shows the calculated breakthrough curves. For $\alpha = 0$, there is flow in only one sub-fracture. As α increases, the fraction of flow moving through the second sub-fracture increases, until for $\alpha = 1$, the two sub-fractures have equal flow. As α increases, the total fracture volume increases, resulting in a delay of the breakthrough curve. The key feature to note is the second peak representing slow-moving tracer in the smaller sub-fracture for $0 < \alpha < 1$. The same general pattern exists for advection-only (no matrix blocks present at all), advection and diffusion only (non-sorbing tracer I), or advection, diffusion, and sorption (strongly sorbing tracer Co). Diffusion and sorption delay all the peak arrivals and also increase the spread among peaks for different tracers. They also make the second peak more distinctive (α=0.1 shows this effect most clearly) because the smaller fracture porosity of the smaller sub-fracture makes diffusion and sorption more important relative to advection than for the larger sub-fracture (see Equations (4), (6), and (12)).

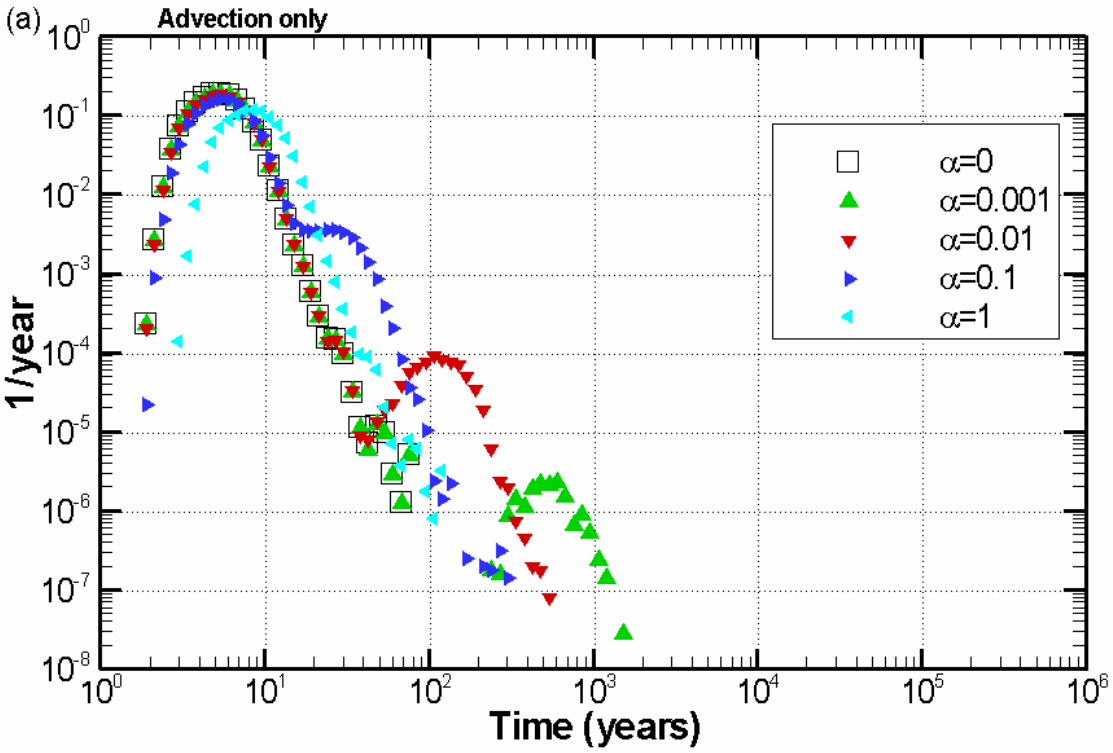
(a)
Advection only
1/year
Time (years)
α=0
α=0.001
α=0.01
α=0.1
α=1

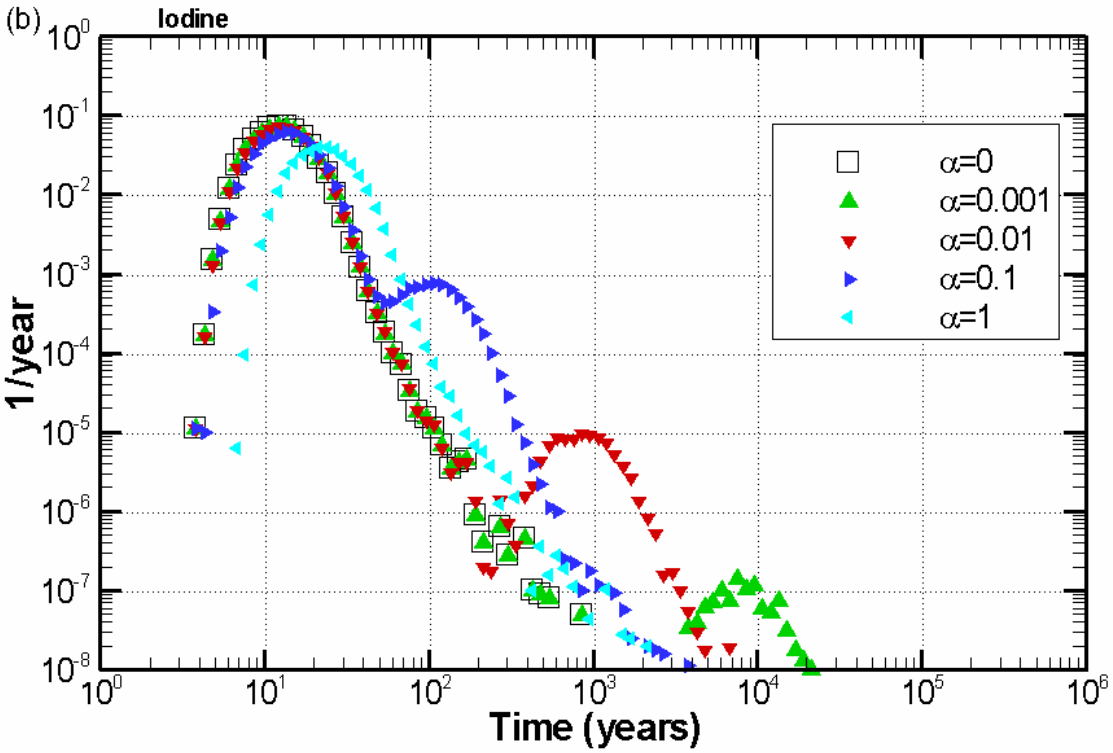
(b)
Iodine
1/year
Time (years)
α=0
α=0.001
α=0.01
α=0.1
α=1

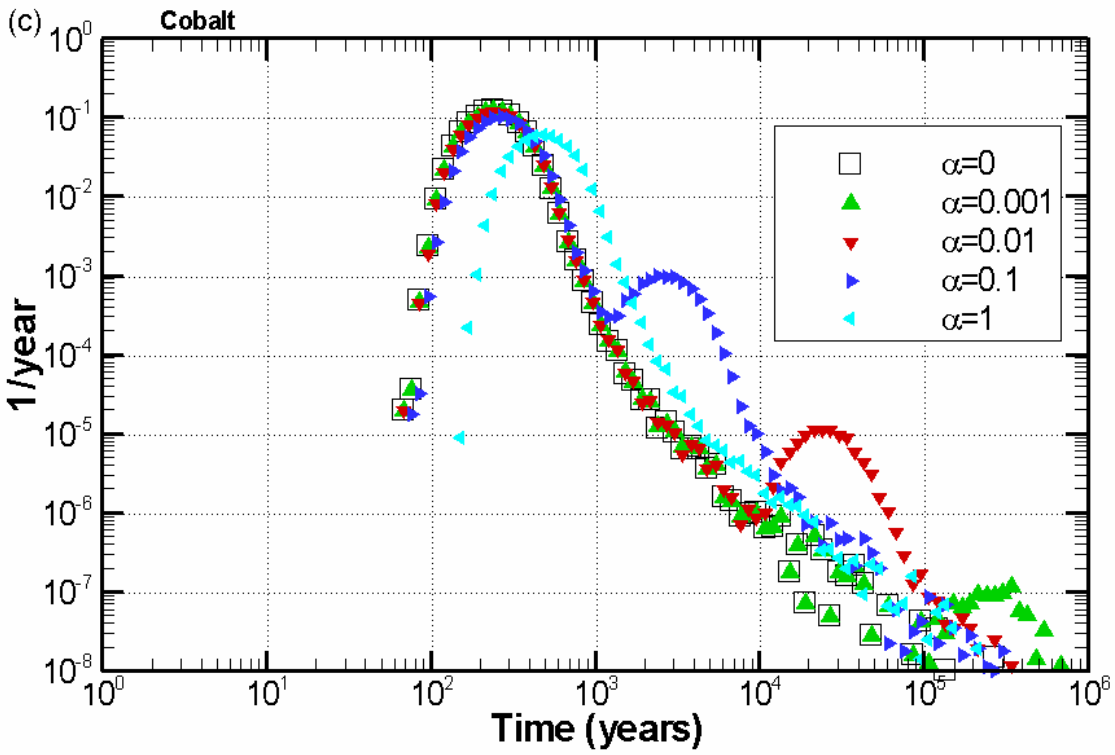

Figure 22. *The effect of α values for (a) advection-only (no diffusion or sorption), (b) a non-sorbing tracer (I), and (c) a moderately sorbing tracer (Co).*

5 Discussion

5.1.1 Conceptual issues

The new approach is shown to be feasible. The results appear to be reasonable, in terms of parameter dependence and sensitivity. The approach includes sufficient physics to account for structure within the complex fracture, such as multiple sub-fractures and smaller gouge and blocks for diffusion and sorption.

We will perform further sensitivity studies, and we will explore the limitations of the current approach. An interesting part of this exercise is to consider how much freedom we still have in choosing parameters, after having matched observed tracer test breakthrough curves.

A related question is how reliable parameters obtained from the Task 6A calibration are for simulating PA behavior. Two factors come into play. First is the great difference between the time scales of the STT-1b tracer test (4 hours to 40 days) and performance assessment tracer arrival times (up to 10,000 years). Second is the effect of fracture plane heterogeneity and the different flow paths activated by the tracer-test and PA boundary conditions. The features of a heterogeneous transmissivity distribution that most strongly impact advective flow paths and travel times are spatial correlation length, mean transmissivity, transmissivity anisotropy ratio, effective fracture porosity, and the variability of the transmissivity distribution.

The transmissivity spatial variation gives rise to flow channeling effects, which affect the so-called “effective flow wetted surface (FWS)” that is an important factor in certain calculational models simulating solute transport retardation due to diffusion and sorption. The relationship between FWS determined from short term tracer tests and appropriate FWS to be used for long term PA is yet to be carefully evaluated. There is a good chance that FWS for PA may be more simply determined: because of potential “diffusion-saturation” of smaller heterogeneity features, their effect becomes a simple retardation factor for long times. Our present method presents a good approach to study the relationship.

5.1.2 Lessons learned

Comparison of the tracer arrival histories for pulse injections for Tasks 6B and 6B2 (Figures 18 and 20) shows that they share many of the same general features. For example, the delay between the arrivals of different tracers is controlled by the sorptive properties, which are the same in both cases. Similarly, the relative importance of diffusion and sorption into different matrix block populations, which controls whether or not the double-hump character of the tracer arrival history is manifested, is the same for both cases. One important difference is the smoother, more regular shapes of the concentration pulses for Task 6B2. This smoothing comes from averaging over the greater number of flow paths that develop under the Task 6B2 boundary conditions.

It is difficult to reconcile the drawdowns observed during the STT-1b tracer test and the transmissivity distribution created stochastically based on parameters inferred from hydraulic testing. Firstly, the stochastic model produces drawdowns that are over one order of magnitude bigger than those observed in the field. Secondly, the presumed spatial correlation lengths for Feature A (0.3 to 0.4 m, from the Task 6B2 specifications) is quite a bit smaller than the distance between observation and production borehole intervals (about 5 m). However, the large difference in drawdown among the observation locations would lead one to believe that the transmissivity correlation length is actually comparable to the borehole spacing. It may be useful to systematically compare previous hydrologic testing of Feature A (Winberg et al., 2000) and the drawdowns measured during the STT-1b tracer test, to ensure that they are internally consistent.

6 References

Deutsch, C.V. and A.G. Journel, GSLIB: Geostatistical Software Library and User's Guide, 2nd Ed., Oxford University Press, New York, 1998.

Mazurek, M., P. Bossart and J. Hermanson, Classification and characterization of water-conducting features at Äspö., *Proc. Intern. Seminar First TRUE Stage,* Äspö Hard Rock Laboratory, Sweden, September 11-13, 2000, published by the Swedish Nuclear Fuel and Waste Management Company (SKB), Stockholm, Sweden, 2001.

Rasmuson, A. and I. Neretnieks, Migration of radionuclides in fissured rock: The influence of micropore diffusion and longitudinal dispersion, Journal of Geophysical Research, 86(B5), 3749-3758, 1981.

Tang, D.H., E.O. Frind, and E.A. Sudicky, Contaminant transport in fracture porous media: Analytical solution for a single fracture, Water Resources Research, 17(3), 555-564, 1981.

Tsang, C.-F. and C. Doughty, An approach to modeling solute transport in a complex fracture, Lawrence Berkeley National Laboratory Report LBNL-50537, 2002.

Tsang, C-F. and C. Doughty, A particle-tracking approach to simulating transport in a complex fracture, Water Resources Research, 39(7), 1174-1178, 2003.

Tsang, Y.W. and C.-F. Tsang, A particle-tracking method for advective transport in fractures with diffusion into finite matrix blocks, Water Resources Research, 37(3), 831-835, 2001.

Winberg, A., P. Andersson, J. Hermanson, J. Byegard, V. Cvetkovic, and L. Birgersson, Aspo Hard Rock Laboratory, Final report of the first stage of the tracer retention understanding experiments, Swedish Nuclear Fuel and Waste Management Co., TR-00-07, 2000.